J. Fluid Mech. (2016), *vol.* 800, *pp.* 720–752.
doi:10.1017/jfm.2016.426

Extension of a viscous thread with temperature-dependent viscosity and surface tension

Dongdong He[1,†], Jonathan J. Wylie[2,6], Huaxiong Huang[3,4,6] and Robert M. Miura[5]

[1]School of Aerospace Engineering and Applied Mechanics, Tongji University, Shanghai 200092, China

[2]Department of Mathematics, City University of Hong Kong, Tat Chee Avenue, Hong Kong

[3]Department of Mathematics and Statistics, York University, Toronto, ON M3J 1P3, Canada

[4]Fields Institute for Research in Mathematical Sciences, Toronto, ON M5T 3J1, Canada

[5]Department of Mathematical Sciences, New Jersey Institute of Technology, Newark, NJ 07102, USA

[6]Center for Applied Mathematics and Statistics, New Jersey Institute of Technology, Newark, NJ 07102, USA

(Received 10 June 2015; revised 4 May 2016; accepted 20 June 2016; first published online 14 July 2016)

We consider the evolution of a long and thin vertically aligned axisymmetric viscous thread that is composed of an incompressible fluid. The thread is attached to a solid wall at its upper end, experiences gravity and is pulled at its lower end by a fixed force. As the thread evolves, it experiences either heating or cooling by its environment. The heating affects the evolution of the thread because both the viscosity and surface tension of the thread are assumed to be functions of the temperature. We develop a framework that can deal with threads that have arbitrary initial shape, are non-uniformly preheated and experience spatially non-uniform heating or cooling from the environment during the pulling process. When inertia is completely neglected and the temperature of the environment is spatially uniform, we obtain analytic solutions for an arbitrary initial shape and temperature profile. In addition, we determine the criteria for whether the cross-section of a given fluid element will ever become zero and hence determine the minimum stretching force that is required for pinching. We further show that the dynamics can be quite subtle and leads to surprising behaviour, such as non-monotonic behaviour in time and space. We also consider the effects of non-zero Reynolds number. If the temperature of the environment is spatially uniform, we show that the dynamics is subtly influenced by inertia and that the location at which the thread will pinch is selected by a competition between three distinct mechanisms. In particular, for a thread with initially uniform radius and a spatially uniform environment but with a non-uniform initial temperature profile, pinching can occur either at the hottest point, at the points near large thermal gradients or at the pulled end, depending on the Reynolds number. Finally, we show that similar results can be obtained for a thread with initially uniform radius and uniform temperature profile but exposed to a spatially non-uniform environment.

Key words: low-Reynolds-number flows, slender-body theory, thermocapillarity

† Email address for correspondence: dongdonghe@tongji.edu.cn

1. Introduction

In recent years, with the advent of optical fibres (Fitt *et al.* 2001), micro-electrodes (Huang *et al.* 2003, 2007), microfluidic devices (X. Gong, 2015, private communication), polymer optical fibres (Argyros 2013) and microscopy (Gallacchi *et al.* 2001), there has been a rapid increase in the development of new fabrication techniques involving components with extremely small scales. A common feature of these techniques is that they use extensional flows to transform relatively large-scale bulk materials into the required small-scale components using extensive stretching. External stretching in these applications is applied either by pulling material at its ends, and/or by allowing the material to fall under gravity.

Stretching of highly viscous threads in an isothermal setting has been widely studied. In particular, there has been extensive work on steady drawing. Early works in this field neglected the effects of surface tension that may potentially lead to pinching. For the drawing of fibres, pinching must be avoided to ensure that sufficiently long fibres can be manufactured. However, in other applications, such as ink-jet printing and pulling micro-electrodes, pinching is desired. Matovich & Pearson (1969) developed a one-dimensional extensional model that can be applied to both Newtonian and non-Newtonian flows. Denn (1980) discussed the relevance of one-dimensional models to experimental studies that involved both glass fibres and polymer melts. Kaye (1991) considered non-steady flow of non-Newtonian fluids and demonstrated that the use of Lagrangian coordinates could significantly simplify the problem. Dewynne, Ockendon & Wilmott (1992) systematically derived the leading-order equations for extensional flows in slender geometries in the absence of inertia, while Dewynne, Howell & Wilmott (1994) performed a similar analysis that included both inertial and gravitational effects. In an isothermal setting, surface tension effects have been included by a number of authors: Yarin, Gospodinov & Roussinov (1994) used a one-dimensional model to study a thin hollow tube and determined conditions for stable drawing. Cummings & Howell (1999) developed a framework that allowed for the study of the evolution of non-axisymmetric fibres with inertia, gravity and surface tension. Fitt *et al.* (2001) derived a one-dimensional model for capillary drawing including surface tension and internal hole overpressure. Stokes *et al.* (2014) developed a method to deal with optical glass fibres with multiple holes. All of these studies did not explicitly deal with thermal effects.

The viscosity of most materials decreases with temperature. Some materials, such as glasses and polymers, can exhibit such dramatic changes in viscosity that their manipulation can only be performed at high temperatures. Industrial processes therefore often involve preheating before any manipulation occurs and may also involve applying external heating during the manipulation.

Although surface tension effects can sometimes be negligible in such processes (Huang *et al.* 2007), they can play a role if the scales involved are sufficiently small. A notable example is the drawing of micro-structured optical fibres in which small holes in the fibre evolve and possibly close up (Stokes *et al.* 2014). For glasses and polymers, the surface tension coefficient also depends on the temperature. The variation of surface tension with temperature is generally not as dramatic as the variation in viscosity. However, for extending threads, we will show that variations in viscosity affect the rate at which thinning or thickening of the thread occurs, whereas changes in surface tension can determine whether the thread thins or thickens. Therefore, changes in surface tension can fundamentally affect the thread dynamics. In this paper, we will investigate a thin thread where both viscosity and surface tension vary with temperature.

A number of authors have considered how thermal effects give rise to changes in viscosity that significantly modify the drawing process. The steady-state problem with thermal effects was first considered by Shah & Pearson (1972*a*), while stability was considered by Shah & Pearson (1972*b*) and Pearson & Shah (1973). Yarin (1986) showed how the effects of cooling can suppress instabilities. Yin & Jaluria (1998) showed how the fibre drawing speed, the furnace temperature and the preform diameter have significant effects on the temperature field in the material. Gospodinov & Yarin (1997) determined stability conditions for non-isothermal flows of hollow fibres. Gupta & Schultz (1998) systematically derived the leading-order approximations to the full Navier–Stokes equations and analysed higher-order corrections. Yin & Jaluria (2000) compared analytical and numerical approaches for a fibre drawing process with relatively large diameter preforms. Forest & Zhou (2001) showed that such flows can have a strong sensitivity to thermal fluctuations. Huang, Miura & Wylie (2008) considered how dopant diffuses during the drawing process for threads with temperature-dependent viscosity. Wylie, Huang & Miura (2007) showed that thermal effects can lead to hysteresis with steady states existing for which the force required to stretch the thread can decrease as the pulling speed is increased. Suman & Kumar (2009) considered how non-isothermal effects can give rise to draw ratio enhancement. Thermally induced variations in viscosity have also been studied in the setting of gravity currents (Vasilyev, Ten & Yuen 2001). Griffiths & Howell (2008) considered non-axisymmetric capillary tube drawing. These studies assumed that the viscosity depends on the temperature, but neglected thermally induced variations in surface tension.

The problem of a thread that is stretched by gravity or by applying a pulling force at its end presents significant challenges for direct numerical simulation as it requires solution of a nonlinear time-dependent free boundary problem that can exhibit singularity formation (in the form of pinching) at an unknown time. In the isothermal setting, significant progress has been made. Wilson (1988) and Stokes, Tuck & Schwartz (2000) provided a one-dimensional theory for a thread extending under its own weight if inertia is negligible. Inertial effects were included in a numerical study by Stokes & Tuck (2004) and a particularly accurate numerical method was determined by Bradshaw-Hajek, Stokes & Tuck (2007). Wylie, Huang & Miura (2011) determined asymptotic solutions for the case of a thread pulled by its ends by a fixed force with inertial effects. Wylie, Huang & Miura (2015) performed a similar analysis for a thread falling under gravity. In the absence of inertia, surface tension effects were included by Stokes, Bradshaw-Hajek & Tuck (2011). However, all of these studies neglected thermal effects. Thermal effects that give rise to changes in viscosity in such initial boundary-value problems have been included by Huang *et al.* (2003, 2007) who developed a one-dimensional model for the formation of glass micro-electrodes. The role played by viscous heating in extensional flows was considered by Wylie & Huang (2007). As was the case for drawing, these studies assumed that the viscosity depended on the temperature, but neglected thermally induced variations in surface tension.

Thermocapillary effects have been the focus of study in a range of situations. There has been a significant amount of work on thin films. Goussis & Kelly (1991) considered the stability of a liquid film flowing down in an inclined heated plane. The case of non-uniform heating was considered by Miladinova, Slavtchev & Lebon (2002). Marangoni effects were analysed in detail by Kalliadasis, Kiyashko & Demekhin (2003*a*) and the Shkadov integral boundary-layer approximation was considered by Kalliadasis, Demekhin & Ruyer-Quil (2003*b*). Scheid *et al.* (2005)

studied the Benney equation with thermocapillary effects. The rupture of a thin film was considered by Tilley & Bowen (2005). Hu, Ben Hadid & Daniel (2008) considered binary liquid films subject to the Soret effect. Samanta (2008) considered flows down a vertical non-uniformly heated wall. D'Alessio, Pascal & Jasmine (2010) considered the problem of gravity-driven laminar flow of a thin layer of fluid down a heated wavy inclined surface. Flow over a heated topography was also studied by Blyth & Bassom (2012). Chinnov & Shatskiy (2014) experimentally studied thermocapillary instabilities for a falling thread. An extensive review on the thin film literature can be found in Craster & Matar (2009). Most thermocapillary studies neglect temperature dependence in the viscosity, but Kabova, Kuznetsov & Kabov (2012) considered films with both temperature-dependent viscosity and surface tension. We note that effects of surface tension on threads and films can be quite different. In particular, the effects of surface tension tend to be stabilizing in the case of films and destabilizing in the case of threads.

Thermocapillary effects in jets have been studied by Mashayek & Ashgriz (1995) who determined conditions for instability and the subsequent formation of satellite drops. Liquid bridges have also been widely studied. Chen, Sheu & Lee (1990) determined the maximum stable length of non-isothermal liquid bridges. Kuhlmann & Rath (1993) studied the steady axisymmetric thermocapillary flow in a cylindrical liquid bridge. Chen, Abbaschian & Steen (2003) showed that thermocapillary effects could suppress the Plateau–Rayleigh instability. In the context of core-annular flows, Dijkstra & Steen (1991) discussed thermocapillary stabilization for the capillary breakup of an annular film. Wei (2005) derived evolution equations to describe the leading-order stability of such flows. However, as far as we are aware, there have been no studies of thermocapillary effects in highly viscous threads.

In this paper, we therefore study a viscous thread that is composed of a fluid whose viscosity and surface tension coefficient depend on temperature. The thread is attached to a solid wall, falls under its weight, is subject to preheating and will also be externally heated or cooled as it is pulled at its free end by a fixed force. This represents a basic framework that allows for the study of extensional flows that are subject to different types of heating (both external heating and preheating) and extensional forces (both gravity and an imposed extensional force). The study is relevant to threads that are heated and/or cooled and have a length scale sufficiently small that surface tension is significant. Using appropriate assumptions, we will develop a long-wavelength model for the mass, momentum and temperature equations (§§ 2 and 3). For zero Reynolds number and a spatially uniform environment, we will derive analytical solutions for the thread evolution for arbitrary initial shape and temperature profiles and show that a surprisingly rich set of phenomena can occur (§ 4). In particular, we will show that there are a number of mechanisms that can lead to non-monotonicity in both space and time in the profiles for the cross-sectional area and temperature. We will also investigate the effects of inertia and show that the location at which the thread will pinch can be influenced by inertia in subtle ways that involve the interaction of three distinct mechanisms (§ 5). In particular, for a thread with initially uniform radius and a spatially uniform environment but with a non-uniform initial temperature profile, pinching can occur either at the hottest point, at the points near large thermal gradients or at the pulled end, depending on the Reynolds number. Similar results can be obtained for a thread with initially uniform radius and uniform temperature profile but with a spatially non-uniform environment.

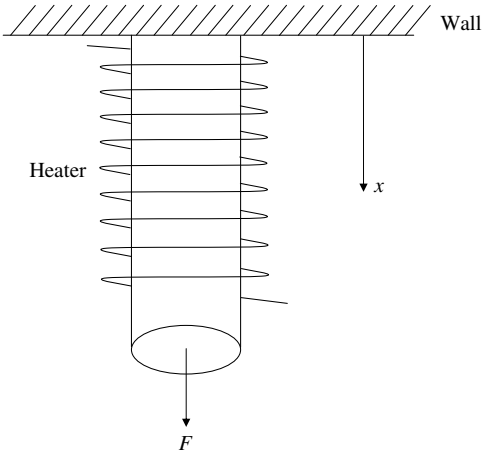

FIGURE 1. Vertical puller with external heater.

2. Formulation

We consider a slender axisymmetric thread of a Newtonian fluid with temperature-dependent viscosity and surface tension. The thread is suspended from a horizontal boundary, experiences gravity and is pulled at its free end by a constant extensional force (figure 1). Prior to stretching, the thread is preheated, and during the stretching process, the thread experiences external heating or cooling from the environment.

We start with the axisymmetric incompressible Navier–Stokes equations and the heat equation as given by Fitt *et al.* (2001)

$$\rho(u_t + uu_x + vu_r) = -p_x + (\boldsymbol{\sigma}_{xx})_x + \frac{1}{r}(r\boldsymbol{\sigma}_{rx})_r + \rho g, \tag{2.1}$$

$$\rho(v_t + uv_x + vv_r) = -p_r + (\boldsymbol{\sigma}_{rx})_x + \frac{1}{r}(r\boldsymbol{\sigma}_{rr})_r - \frac{\boldsymbol{\sigma}_{\phi\phi}}{r}, \tag{2.2}$$

$$u_x + \frac{1}{r}(rv)_r = 0, \tag{2.3}$$

$$\rho c_p(\theta_t + u\theta_x + v\theta_r) = k\left(\frac{1}{r}(r\theta_r)_r + \theta_{xx}\right), \tag{2.4}$$

where t is time, x is the distance measured along the axis of the thread, r is the distance measured radially outward from the centre of the thread, u is the velocity in the x direction, v is the velocity in the r direction, θ is the temperature, ρ is the density of fluid, p is the pressure relative to the ambient air pressure, g is gravity (which is acting in the axial direction), k is the thermal conductivity and c_p is the specific heat capacity. For optically transparent materials (such as glasses) that are subjected to radiative heating, equation (2.4) may not be a reasonable assumption as radiative energy may be absorbed in the interior of the thread. However, given a model for heat flux, see for example, Taroni *et al.* (2013), we will still, in principle, be able to use a broadly similar approach to the one we will use in this paper. The viscous stress components are given by

$$\left.\begin{aligned} \boldsymbol{\sigma}_{xx} = 2\mu(\theta)u_x, \quad \boldsymbol{\sigma}_{rr} = 2\mu(\theta)v_r, \quad \boldsymbol{\sigma}_{rx} = \boldsymbol{\sigma}_{xr} = \mu(\theta)(u_r + v_x), \\ \boldsymbol{\sigma}_{\phi\phi} = \frac{2\mu(\theta)v}{r}, \quad \boldsymbol{\sigma}_{r\phi} = \boldsymbol{\sigma}_{\phi r} = 0, \quad \boldsymbol{\sigma}_{z\phi} = \boldsymbol{\sigma}_{\phi z} = 0, \end{aligned}\right\} \tag{2.5}$$

where ϕ is the angle measured around the axis of the thread and μ is the dynamic viscosity of fluid, which depends on the temperature θ.

The viscosity of the air is negligible compared to the viscosity of the thread, so on the free surface of the thread, there is a balance between the fluid stress and surface tension in the normal and tangential directions

$$\boldsymbol{n}\cdot(-p\boldsymbol{I}+\boldsymbol{\sigma})\cdot\boldsymbol{n}=-\gamma(\theta)\kappa \quad \text{on } r=R(x,t), \tag{2.6}$$

$$\boldsymbol{\tau}\cdot(-p\boldsymbol{I}+\boldsymbol{\sigma})\cdot\boldsymbol{n}=\nabla_s\gamma(\theta)\cdot\boldsymbol{\tau} \quad \text{on } r=R(x,t), \tag{2.7}$$

where $R(x,t)$ is the radius of the thread, $\boldsymbol{I}$ is the identity matrix, $\boldsymbol{\sigma}$ is the viscous stress tensor with components given by (2.5), γ is the surface tension coefficient and κ is the mean curvature of the free surface, given by

$$\kappa=\frac{1}{R(1+R_x^2)^{1/2}}-\frac{R_{xx}}{(1+R_x^2)^{3/2}}. \tag{2.8}$$

In (2.7), ∇_s is the surface gradient, given by $\nabla_s=(\boldsymbol{I}-\boldsymbol{nn})\cdot\nabla$, where $\nabla=(\partial_x,\partial_r,(1/r)\partial_\phi)^{\mathrm{T}}$. The vectors $\boldsymbol{n}$ and $\boldsymbol{\tau}$ are the unit vectors on the free surface in the outward normal and tangential directions, given by

$$\boldsymbol{n}=\frac{1}{\sqrt{1+R_x^2}}(-R_x,1,0)^{\mathrm{T}} \quad \text{and} \quad \boldsymbol{\tau}=\frac{1}{\sqrt{1+R_x^2}}(1,R_x,0)^{\mathrm{T}}, \tag{2.9a,b}$$

respectively. Here the three components of the above vectors are in the x, r and ϕ directions, respectively. In addition, on the free surface, the kinematic condition is

$$R_t+uR_x=v \quad \text{on } r=R(x,t). \tag{2.10}$$

At the upper boundary, we impose a zero normal velocity condition and at the lower boundary we impose a fixed extensional force, F. In fact, when solving the full Navier–Stokes equations, one typically requires two boundary conditions at both ends. However, in this paper we will use long-wavelength asymptotics that represent a singular perturbation of the Navier–Stokes equations and thus only require one boundary condition at each end. At both ends of the thread, there will be thin boundary layers in which the solutions to the long-wavelength equations rapidly adjust to accommodate the neglected boundary conditions.

At the centreline of the thread, there is no heat flux, no viscous stress and no mass flux, so we have

$$r\theta_r\to 0, \quad \mu(\theta)ru_r\to 0, \quad rv\to 0, \quad \text{as } r\to 0. \tag{2.11a–c}$$

Additionally, there is a heat flux balance at the free surface. In general, the heat flux coming from the environment will include both radiative and convective components and can be a complicated function of x and θ that we denote by $-H(x,\theta)$. Then, the heat flux condition on the free surface is

$$-k\boldsymbol{n}\cdot\nabla\theta=-H(x,\theta) \quad \text{on } r=R(x,t). \tag{2.12}$$

Different heat transfer models apply in different temperature ranges. For example, in glass manufacture, which can require heater temperatures in excess of 1000 °C (Kostecki *et al.* 2014), radiative transfer will be dominant. Whereas, for polymer

processing, which generally occurs at significantly lower temperatures, heat transfer is often modelled using the Newtonian law (Denn 2014). We will attempt to present our analysis for a general heating model, but it sometimes proves convenient to specify a particular model. In such cases, we will use Newton's heat transfer law

$$H(x, \theta) = h_w(\theta_h(x) - \theta) \quad \text{on } r = R(x, t), \tag{2.13}$$

where h_w is the heat transfer coefficient and the function $\theta_h(x)$ represents the temperature of the external heater. This formulation also allows for external cooling, which occurs if θ_h is less than θ.

Finally, we must adopt models for the temperature dependence of the viscosity and the surface tension. For materials such as polymers and glasses, the viscosity decreases dramatically with temperature. Temperature increases of approximately 200 °C can induce viscosity decreases of 1–3 orders of magnitude for typical polymers (Wang & Porter 1995; Kalpakjian & Schmid 2007) and can induce viscosity decreases of 2–3 orders of magnitude for typical glasses near the working point (Seward III & Vascott 2005; Fluegel 2007; Bingham 2010). For most materials, the variation of surface tension is not as dramatic as the viscosity, but can still be significant. For example, some silicone oils exhibit a decrease of surface tension of more than 35 % when the temperature increases from 20 to 150 °C (Roe 1968), and polyethylene exhibits a decrease of more than 25 % when the temperature increases from 20 to 180 °C (Wu 1969). Typical glasses exhibit a decrease of approximately 10 % when the temperature increases by 400 °C (Bansal & Doremus 1986). Changes in surface tension are significantly smaller than changes in viscosity, thus many authors neglect variations in surface tension. However, we will show that changes in viscosity affect the time scale of the thread evolution, whereas changes in surface tension can determine whether a thread thins or thickens. Therefore, even relatively modest changes in surface tension can have important consequence for the thread dynamics.

We will model the viscosity–temperature relation using an exponential law, given by

$$\mu(\theta) = \hat{\mu} \mathrm{e}^{-\beta(\theta - \hat{\theta})}, \tag{2.14}$$

where β is a positive constant representing how rapidly the viscosity decreases with temperature, $\hat{\theta}$ is a characteristic initial temperature and $\hat{\mu}$ is the viscosity at the initial characteristic temperature. This model is widely used in the polymer and glass literature (Vlachopoulos 2003; Huang *et al.* 2007; Vlachopoulos & Polychronopoulos 2012). We will model the surface-tension–temperature relation using a linear function, given by

$$\gamma(\theta) = \hat{\gamma}(1 - \alpha(\theta - \hat{\theta})), \tag{2.15}$$

where α is a positive constant representing how rapidly the surface tension decreases with temperature and $\hat{\gamma}$ is the surface tension at the initial characteristic temperature. This model is also widely used in the polymer and glass literature (Roe 1968; Wu 1969, 1970; Bansal & Doremus 1986). We note that, for most materials, $\beta > \alpha$, that is, the variation of viscosity with temperature is more rapid than the variation of surface tension.

We denote the initial length of the thread as l and the initial characteristic radius of the thread as $\hat{R}$. We denote the characteristic temperature difference as $\bar{\theta}$. In the case of heating, $\bar{\theta}$ will be the characteristic difference between the initial temperature of the thread and the heater. In the case of cooling, $\bar{\theta}$ will be the characteristic difference between the initial temperature of the thread and the environment.

We non-dimensionalize the above equations (2.1)–(2.5) and conditions (2.6)–(2.13) using the following scales:

$$\left.\begin{gathered} x = lx', \quad r = \hat{R}r', \quad R = \hat{R}R', \quad t = \frac{3\hat{R}\hat{\mu}}{\sqrt{\pi}\hat{\gamma}}t', \quad u = \frac{\sqrt{\pi}\hat{\gamma}l}{3\hat{\mu}\hat{R}}u', \quad v = \frac{\sqrt{\pi}\hat{\gamma}}{3\hat{\mu}}v', \\ \theta = \hat{\theta} + \bar{\theta}\theta', \quad \theta_h(x) = \hat{\theta} + \bar{\theta}\theta_h'(x), \quad p = \frac{\sqrt{\pi}\hat{\gamma}}{3\hat{R}}p', \quad \mu = \hat{\mu}\mu', \quad \gamma = \hat{\gamma}\gamma'. \end{gathered}\right\} \tag{2.16}$$

After substituting the above scalings and dropping primes, the resulting non-dimensional equations for (2.1)–(2.4) are

$$\begin{aligned} 3Re\varepsilon^2(u_t + uu_x + vu_r) \;=\; & -\varepsilon^2 p_x + \frac{1}{r}(\mu(\theta)ru_r)_r + \varepsilon^2(2\mu(\theta)u_x)_x \\ & + \frac{\varepsilon^2}{r}(\mu(\theta)rv_x)_r + 3\varepsilon^2 Bo, \end{aligned} \tag{2.17}$$

$$3Re\varepsilon^2(v_t + uv_x + vv_r) = -p_r + (\mu(\theta)u_r)_x + \varepsilon^2(\mu(\theta)v_x)_x + \frac{1}{r}(2r\mu(\theta)v_r)_r - \frac{2\mu(\theta)v}{r^2}, \tag{2.18}$$

$$u_x + \frac{1}{r}(rv)_r = 0, \tag{2.19}$$

$$Pe\varepsilon^2(\theta_t + u\theta_x + v\theta_r) = \frac{1}{r}(r\theta_r)_r + \varepsilon^2\theta_{xx}, \tag{2.20}$$

where

$$\varepsilon = \frac{\hat{R}}{l}, \quad Pe = \frac{\sqrt{\pi}\rho c_p\hat{\gamma}l^2}{3\hat{\mu}k\hat{R}}, \quad Re = \frac{\sqrt{\pi}\rho\hat{\gamma}l^2}{9\hat{\mu}^2\hat{R}}, \quad Bo = \frac{\rho g\hat{R}l}{\sqrt{\pi}\hat{\gamma}}. \tag{2.21a–d}$$

Here, ε is the aspect ratio, Pe is the Peclet number that compares along-thread advection with along-thread conduction, Re is the Reynolds number that compares the relative importance of inertial and viscous effects and Bo is the Bond number that compares the gravitational and surface tension forces.

On the thread surface, the dimensionless normal and tangential stress conditions are

$$\begin{aligned} & -p + \frac{1}{1+\varepsilon^2R_x^2}(2\mu(\theta)v_r - 2\mu(\theta)R_xu_r + \varepsilon^2(2\mu(\theta)u_xR_x^2 - 2\mu(\theta)R_xv_x)) \\ & \quad = -\frac{3\gamma(\theta)}{\sqrt{\pi}}\left(\frac{1}{R(1+\varepsilon^2R_x^2)^{1/2}} - \frac{\varepsilon^2R_{xx}}{(1+\varepsilon^2R_x^2)^{3/2}}\right) \quad \text{on } r = R(x,t), \end{aligned} \tag{2.22}$$

$$\begin{aligned} & \mu(\theta)u_r + \varepsilon^2(\mu(\theta)v_x + 2\mu(\theta)R_xv_r - 2\mu(\theta)R_xu_x - \mu(\theta)u_rR_x^2) - \varepsilon^4\mu(\theta)R_x^2v_x \\ & \quad = \frac{3\varepsilon^2(1+\varepsilon^2R_x^2)^{1/2}(\gamma(\theta))_x}{\sqrt{\pi}} \quad \text{on } r = R(x,t). \end{aligned} \tag{2.23}$$

The non-dimensional kinematic boundary condition is,

$$R_t + uR_x = v \quad \text{on } r = R(x,t). \tag{2.24}$$

The non-dimensional regularity conditions at the centreline are

$$r\theta_r \to 0, \quad \mu(\theta)ru_r \to 0, \quad rv \to 0, \quad \text{as } r \to 0. \tag{2.25a–c}$$

The non-dimensional heat flux condition for Newton's law is

$$\frac{\theta_r - \varepsilon^2 R_x \theta_x}{\sqrt{1+\varepsilon^2 R_x^2}} = \frac{\varepsilon^2 Pe\mathscr{H}}{2\sqrt{\pi}}(\theta_h(x) - \theta) \quad \text{on } r = R(x,t), \tag{2.26}$$

where

$$\mathscr{H} = \frac{6\hat{\mu} h_w}{\rho c_p \hat{\gamma}}. \tag{2.27}$$

Here, $\mathscr{H}$ is a dimensionless number that compares the external heat flux with along-thread advection.

Following many previous studies (Fitt *et al.* 2001; Stokes & Tuck 2004; Huang *et al.* 2007, 2008; Stokes *et al.* 2011), we proceed by assuming that the aspect ratio is small, and posing the following asympotic expansions

$$\theta = \theta^{(0)} + \varepsilon^2\theta^{(1)} + \varepsilon^4\theta^{(2)} + \cdots, \tag{2.28}$$
$$u = u^{(0)} + \varepsilon^2 u^{(1)} + \varepsilon^4 u^{(2)} + \cdots, \tag{2.29}$$
$$v = v^{(0)} + \varepsilon^2 v^{(1)} + \varepsilon^4 v^{(2)} + \cdots, \tag{2.30}$$
$$p = p^{(0)} + \varepsilon^2 p^{(1)} + \varepsilon^4 p^{(2)} + \cdots. \tag{2.31}$$

It proves to be convenient to start by analysing the non-dimensional heat equation (2.20) and show that, under an appropriate approximation, the leading-order temperature profile is independent of the radial coordinate.

Substituting (2.28)–(2.30) into (2.20), (2.25)–(2.26) and formally retaining only $O(1)$ terms, we obtain

$$\frac{1}{r}(r\theta_r^{(0)})_r = 0, \tag{2.32}$$
$$r\theta_r^{(0)} \to 0 \quad \text{as } r \to 0, \tag{2.33}$$
$$\theta_r^{(0)} = 0 \quad \text{on } r = R(x,t). \tag{2.34}$$

From (2.32) to (2.34), we immediately see that $\theta^{(0)}$ is a function of x and t only. Hence, at the next order, (2.20), (2.25) and (2.26) give

$$Pe(\theta_t^{(0)} + u^{(0)}\theta_x^{(0)}) = \frac{1}{r}(r\theta_r^{(1)})_r + \theta_{xx}^{(0)}, \tag{2.35}$$
$$r\theta_r^{(1)} \to 0 \quad \text{as } r \to 0, \tag{2.36}$$
$$\theta_r^{(1)} - R_x\theta_x^{(0)} = \frac{Pe\mathscr{H}}{2\sqrt{\pi}} H(x, \theta^{(0)}) \quad \text{on } r = R(x,t), \tag{2.37}$$

where

$$H(x,\theta) = \theta_h - \theta. \tag{2.38}$$

We note that $H(x,\theta) > 0$ corresponds to heating while $H(x,\theta) < 0$ corresponds to cooling.

The leading-order temperature, $\theta^{(0)}$, does not depend on the radial coordinate r and so, at leading order, the viscosity is also independent of r. Moreover, the leading-order approximation for (2.17) gives

$$\frac{1}{r}(\mu(\theta^{(0)})ru_r^{(0)})_r = 0. \tag{2.39}$$

Integrating the above equation and using the leading-order regularity conditions (2.25), it is readily seen that the leading-order velocity, $u^{(0)}$, is also independent of r. Hence, we can integrate (2.35) and apply the boundary conditions (2.37) to obtain

$$\theta_t^{(0)} + u^{(0)}\theta_x^{(0)} = \frac{\mathscr{H}H(x,\theta^{(0)})}{\sqrt{A}} + \frac{1}{PeA}(A\theta_x^{(0)})_x, \tag{2.40}$$

where $A = \pi R^2$ is the dimensionless cross-sectional area of the thread.

Having shown that the leading-order temperature, and hence the viscosity, are independent of r, the derivation of the leading-order long-wave momentum and continuity equations is broadly similar to Fitt *et al.* (2001), except that an extra surface tension derivative term appears in the force balance in the tangential direction at the free surface. We therefore only briefly derive these equations and refer the reader to Fitt *et al.* (2001) for a detailed derivation.

Using the leading-order continuity equation (2.19) and the leading-order r-momentum equation (2.18), it can be readily seen that the leading-order pressure, $p^{(0)}$, is independent of r and the following relation is valid

$$v^{(0)} = -\frac{r}{2}u_x^{(0)}. \tag{2.41}$$

The leading-order normal stress condition gives,

$$-p^{(0)} + 2\mu(\theta^{(0)})v_r^{(0)} = -\frac{3}{\sqrt{\pi}}\frac{\gamma(\theta^{(0)})}{R} \quad \text{on } r = R(x,t). \tag{2.42}$$

In addition, the first-order x-momentum equation (2.17) gives

$$3Re(u_t^{(0)} + u^{(0)}u_x^{(0)}) = -p_x^{(0)} + \frac{1}{r}(\mu(\theta^{(0)})ru_r^{(1)})_r + (2\mu(\theta^{(0)})u_x^{(0)})_x + \frac{1}{r}(\mu(\theta^{(0)})rv_x^{(0)})_r + 3Bo. \tag{2.43}$$

The first-order tangential condition (2.23) on the free surface yields

$$\begin{aligned}&\mu(\theta^{(0)})u_r^{(1)} + \mu(\theta^{(0)})v_x^{(0)} + 2\mu(\theta^{(0)})R_xv_r^{(0)} - 2\mu(\theta^{(0)})R_xu_x^{(0)}\\ &\quad = \frac{3}{\sqrt{\pi}}(\gamma(\theta^{(0)}))_x \quad \text{on } r = R(x,t).\end{aligned} \tag{2.44}$$

All of the above equations (2.41)–(2.44) are the same as Fitt *et al.* (2001) except for (2.44), which has an extra term $3/\sqrt{\pi}(\gamma(\theta^{(0)}))_x$ due to the variation of the surface tension coefficient on the free surface.

Multiplying (2.43) by r, integrating over r and using (2.41), (2.42) and (2.44), one can obtain the following leading-order momentum equation

$$Re(u_t^{(0)} + u^{(0)}u_x^{(0)}) = \frac{1}{R^2}(\mu(\theta^{(0)})R^2u_x^{(0)})_x - \frac{1}{\sqrt{\pi}}\left(\frac{\gamma(\theta^{(0)})}{R}\right)_x + \frac{2}{\sqrt{\pi}}\frac{(\gamma(\theta^{(0)}))_x}{R} + Bo. \tag{2.45}$$

After some simple calculations, the second and third terms on the right-hand side of (2.45) can be combined into a single term. Hence (2.45) yields

$$Re(u_t^{(0)} + u^{(0)}u_x^{(0)}) = \frac{1}{A}(\mu(\theta^{(0)})Au_x^{(0)})_x + \frac{1}{A}(\gamma(\theta^{(0)})\sqrt{A})_x + Bo. \tag{2.46}$$

Moreover, the mass conservation equation can be easily obtained by substituting (2.41) into the dimensionless kinematic boundary condition (2.24), which is given by

$$A_t + (Au^{(0)})_x = 0. \tag{2.47}$$

For notational brevity we drop the superscript zero and obtain the following leading-order system for the mass, momentum and heat equations

$$A_t + (Au)_x = 0, \tag{2.48}$$

$$Re(u_t + uu_x) = \frac{1}{A}(\mu(\theta)Au_x + \gamma(\theta)\sqrt{A})_x + Bo, \tag{2.49}$$

$$\theta_t + u\theta_x = \frac{\mathscr{H}H(x,\theta)}{\sqrt{A}} + \frac{1}{PeA}(A\theta_x)_x. \tag{2.50}$$

The above derivation has been performed for conductive heat transfer in the interior of the thread and Newton's model for heat transfer on the free surface, but if other models of heat transfer are adopted, only the right-hand side of (2.50) will be affected. We note that, even as pinching is approached, these long-wavelength equations precisely capture the relevant contributions to the Navier–Stokes equation (Eggers 1993).

In addition, the dimensionless functions describing the temperature variation of viscosity and surface tension are

$$\mu(\theta) = \mathrm{e}^{-b\theta} \quad \text{and} \quad \gamma(\theta) = 1 - a\theta, \tag{2.51a,b}$$

respectively, where

$$b = \beta\bar{\theta}, \quad a = \alpha\bar{\theta}. \tag{2.52a,b}$$

Equations (2.48)–(2.50) are also subject to initial and boundary conditions. In this paper, we will consider the following conditions. Initially, the thread has an arbitrary shape, an arbitrary temperature profile and zero velocity, that is

$$A(x,0) = A_0(x), \quad \theta(x,0) = \theta_0(x) \quad \text{and} \quad u(x,0) = 0. \tag{2.53a–c}$$

At the free end of the thread, there is a constant extensional force

$$\mu(\theta)Au_x + \gamma(\theta)\sqrt{A} = \mathscr{F} \quad \text{at } x = \ell(t), \tag{2.54}$$

where

$$\mathscr{F} = \frac{F}{\sqrt{\pi}\hat{\gamma}\hat{R}}, \tag{2.55}$$

and $\mathscr{F}$ compares the imposed extensional force and surface tension force. Here $\ell(t)$ is the location of the free end of the thread which must be obtained by solving

$$\frac{\mathrm{d}\ell}{\mathrm{d}t} = u(\ell(t), t). \tag{2.56}$$

At the upper boundary, the zero velocity condition applies,

$$u = 0 \quad \text{at } x = 0. \tag{2.57}$$

We will further assume that the thread is initially located between $x = 0$ and $x = 1$, so that (2.56) has the initial condition $\ell(0) = 1$.

In order to have an idea of the order of magnitude of the various dimensionless quantities in a realistic setting, we consider scales that are appropriate for polymer processing (Roe 1968; Wu 1969, 1970; Vlachopoulos 2003; Vlachopoulos & Polychronopoulos 2012; Ashby & Jones 2013; Denn 2014)

$$\left.\begin{gathered}\hat{\theta}\sim 10^2\ \text{K},\quad \rho\sim 10^3\ \text{kg m}^{-3},\quad \hat{R}\sim 10^{-4}\ \text{m},\quad l\sim 10^{-2}\ \text{m},\quad \hat{\gamma}\sim 10^{-2}\ \text{N m}^{-1},\\ \hat{\mu}\sim 10^2\ \text{kg m}^{-1}\ \text{s}^{-1},\quad c_p\sim 10^3\ \text{J K}^{-1}\ \text{kg}^{-1},\quad k\sim 1\ \text{W m}^{-1}\ \text{K}^{-1},\\ h_w\sim 10\ \text{W m}^{-2}\ \text{K}^{-1},\quad \bar{\theta}\sim 10^2\ \text{K}.\end{gathered}\right\} \tag{2.58}$$

In different applications, the applied extensional force can take widely varying values. For example, the force is zero in purely gravity-driven extrusion, while the force may be very large if extremely rapid stretching is required. We will consider the case in which the force is of comparable order to the weight of the thread, namely $F\sim 10^{-6}$ N. In addition, for most polymers, $\alpha\hat{\gamma}$ has the order from 10^{-5} m^{-1} K^{-1} to 10^{-4} N m^{-1} K^{-1} (Roe 1968; Wu 1969, 1970), while β typically has the order from 10^{-2} K^{-1} to 10^{-1} K^{-1} (Vlachopoulos 2003; Vlachopoulos & Polychronopoulos 2012).

These scales give the following order-of-magnitude estimates for the dimensionless parameters:

$$\left.\begin{gathered}Pe=O(10^2),\quad \varepsilon=O(10^{-2}),\quad Re=O(10^{-3}),\quad Bo=O(1),\\ \mathscr{F}=O(1),\quad a=O(10^{-1})-O(1),\quad b=O(1)-O(10),\quad \mathscr{H}=O(1).\end{gathered}\right\} \tag{2.59}$$

The size of the axial diffusion term in (2.50) is Pe^{-1}, which is $O(10^{-2})$ and hence is small, and we will neglect it in what follows. For any small non-zero Re, Wylie *et al.* (2011) have shown that if A becomes sufficiently small, then inertial effects cannot be neglected. We will therefore retain the inertial terms. As mentioned, for most materials, the variation of viscosity with temperature is more rapid than the variation of surface temperature, and this implies $b>a$. Broadly similar estimates can be obtained for glass manufacturing at very high temperatures between the working point and the melting point where its viscosity is 10–10^3 Pa s (Bingham 2010).

We note that the above derivation assumes a Newtonian fluid. Of course, some polymers can exhibit viscoelastic behaviour under certain flow conditions. However, Ashby & Jones (2013) pointed out that typical linear polymers are well approximated as a Newtonian viscous fluid for temperatures above 100 °C. Moreover, viscoelastic effects are generally neglected for polyester and nylon processing (Denn 2014), and we will therefore neglect viscoelastic effects in this paper. We note that the derivation of (2.48)–(2.50) requires $\varepsilon^2 Pe\ll 1$ and $\varepsilon^2 Re\ll 1$.

3. Lagrangian form of the model equations

We transform the above system from Eulerian coordinates $(x,\,t)$ into Lagrangian coordinates $(\xi,\,\tau)$, where $\tau=t$ is time. Each fluid element is labelled by its initial location ξ and fluid elements travel with fluid velocity $x_\tau=u$. Then,

$$\frac{\partial}{\partial\tau}=\frac{\partial}{\partial t}+u\frac{\partial}{\partial x} \tag{3.1}$$

and

$$\frac{\partial}{\partial\xi}=\frac{\partial x}{\partial\xi}\frac{\partial}{\partial x}. \tag{3.2}$$

The initial conditions are given by

$$A(\xi, 0) = A_0(\xi), \quad u(\xi, 0) = 0, \quad \theta(\xi, 0) = \theta_0(\xi), \quad x(\xi, 0) = \xi. \tag{3.3a–d}$$

Applying (3.1)–(3.2) to the conservation of mass (2.48), we obtain

$$A_\tau + A\frac{u_\xi}{x_\xi} = 0. \tag{3.4}$$

Using $u = x_\tau$, (3.4) can be rewritten as $(Ax_\xi)_\tau = 0$. Integrating with respect to τ and applying the initial condition (3.3), we obtain $Ax_\xi = A_0$. Thus, (3.2) becomes

$$\frac{\partial}{\partial \xi} = \frac{A_0}{A}\frac{\partial}{\partial x}, \tag{3.5}$$

and so (2.48)–(2.50) become

$$A_\tau + \frac{A^2}{A_0}u_\xi = 0, \tag{3.6}$$

$$Reu_\tau = \frac{1}{A_0}(-\mu(\theta)A_\tau + \gamma(\theta)\sqrt{A})_\xi + Bo, \tag{3.7}$$

$$\theta_\tau = \frac{\mathscr{H}H(x, \theta)}{\sqrt{A}}. \tag{3.8}$$

In order to compute the location of a given fluid element, one must solve

$$x_\xi = \frac{A_0}{A}. \tag{3.9}$$

At the upper boundary, the zero velocity condition is

$$u = 0 \quad \text{at } \xi = 0. \tag{3.10}$$

Transforming the free boundary condition (2.54) into Lagrangian coordinates and recalling that the free end of the thread is at $\xi = 1$, we obtain

$$-\mu(\theta)A_\tau + \gamma(\theta)\sqrt{A} = \mathscr{F} \quad \text{at } \xi = 1, \tag{3.11}$$

which states that the stretching force at the free end of the thread is $\mathscr{F}$.

4. Analytical solutions for zero inertia with a spatially uniform heater

We now consider the case of arbitrary initial shape $A_0(\xi)$, arbitrary initial temperature profile $\theta_0(\xi)$, zero inertia $Re = 0$ and a spatially uniform heater $H(x, \theta) = H(\theta)$. In this case, the cross-sectional area and temperature for each fluid element evolve independently of all other fluid elements and we can obtain analytical solutions. Neglecting the inertial term by setting $Re = 0$ in (3.7), we can integrate with respect to ξ and after using the boundary condition (3.11), we obtain

$$A_\tau = \frac{\gamma(\theta)\sqrt{A} - \mathscr{F}^*(\xi)}{\mu(\theta)} \quad \text{for } 0 \leqslant \xi \leqslant 1, \tag{4.1}$$

where

$$\mathscr{F}^*(\xi) = \mathscr{F} + Bo\int_\xi^1 A_0(\xi')\,\mathrm{d}\xi'. \tag{4.2}$$

Examining (4.1), we easily see that viscosity affects the time scale of the thread evolution but not the sign of A_τ, whereas the surface tension coefficient can determine the sign of A_τ, that is whether the thread thins or thickens. Thus, even relatively modest changes in surface tension can have important consequence for the thread dynamics.

Since $H(x, \theta) = H(\theta)$, equation (3.8) becomes

$$\theta_\tau = \frac{\mathscr{H} H(\theta)}{\sqrt{A}}. \tag{4.3}$$

Dividing (4.1) by (4.3) we obtain a Bernoulli-type ordinary differential equation

$$\frac{\partial A}{\partial \theta} = 2g(\theta)A - 2\mathscr{F}^*(\xi)h(\theta)\sqrt{A}, \tag{4.4}$$

where

$$g(\theta) = \frac{\gamma(\theta)}{2\mu(\theta)\mathscr{H} H(\theta)} \quad \text{and} \quad h(\theta) = \frac{1}{2\mu(\theta)\mathscr{H} H(\theta)}. \tag{4.5a,b}$$

The solution of (4.4) subject to the boundary condition (3.3) is

$$A = \exp\left[2\int_{\theta_0(\xi)}^{\theta} g(\theta')\,\mathrm{d}\theta'\right]\left\{\sqrt{A_0(\xi)} - \mathscr{F}^*(\xi)G(\theta, \theta_0(\xi))\right\}^2, \tag{4.6}$$

where

$$G(\theta, \theta_0(\xi)) = \int_{\theta_0(\xi)}^{\theta} h(\theta')\exp\left[-\int_{\theta_0(\xi)}^{\theta'} g(\theta'')\,\mathrm{d}\theta''\right]\mathrm{d}\theta'. \tag{4.7}$$

For the case of heating ($H > 0$), θ will be an increasing function of time. Whereas, for the case of cooling ($H < 0$), θ will be a decreasing function of time. Therefore, in both cases, the expression $G(\xi, \theta)$ defined in (4.7) is an increasing function of time. We also note that $G(\xi, \theta)$ is zero at $\tau = 0$. Equation (4.6) reflects the fact that the cross-section varies due to two mechanisms. First, the cross-section tends to increase due to surface tension. This is reflected in the exponential term which increases monotonically. Second, the cross-section tends to decrease as a result of gravity and the imposed fulling force. This is reflected in the $\mathscr{F}^*(\xi)G(\theta', \theta_0(\xi))$ term. In some sense, G represents the relative importance of thinning (due to gravity and the imposed fulling force) and broadening (due to surface tension). We note that if expressed in dimensional terms, G^{-1} has the same units as surface tension.

Substituting (4.6) into (4.3), we obtain a separable equation that has solution

$$\tau = \int_{\theta_0(\xi)}^{\theta} \frac{1}{\mathscr{H} H(\theta')}\exp\left[\int_{\theta_0(\xi)}^{\theta'} g(\theta'')\,\mathrm{d}\theta''\right]\left\{\sqrt{A_0(\xi)} - \mathscr{F}^*(\xi)G(\theta', \theta_0(\xi))\right\}\mathrm{d}\theta'. \tag{4.8}$$

For each fluid element (labelled by ξ), equation (4.6) gives A as a function of θ and ξ while (4.8) gives τ as a function of θ and ξ. Therefore, when combined, (4.6) and (4.8) implicitly define A and θ as functions of ξ and τ.

4.1. *Dynamics of a single fluid element*

We now consider the various types of behaviour that (4.6) and (4.8) can exhibit. In analysing these two equations, it is important to note that if the cross-sectional area A of any of the fluid elements were to become zero, then the thread would experience a topological change and the two ends of the thread would no longer be connected to one another. If this were to occur, the thread would no longer transmit the extensional force $\mathscr{F}$ throughout its length and so (4.1) would no longer be valid. In fact, for any small non-zero Re, Wylie *et al.* (2011) have shown that if A becomes sufficiently small, then the inertial effects cannot be neglected. Hence, the following analysis will only be valid as long as A is sufficiently large for all fluid elements.

4.1.1. *Early time dynamics*

The early time behaviour of (4.6) and (4.8) is straightforward to address using (4.1). If $\mathscr{F}^*(\xi) < \gamma(\theta_0(\xi))\sqrt{A_0(\xi)}$, then A will initially increase, whereas if $\mathscr{F}^*(\xi) > \gamma(\theta_0(\xi))\sqrt{A_0(\xi)}$, then A will initially decrease. In the case $\mathscr{F}^*(\xi) = \gamma(\theta_0(\xi))\sqrt{A_0(\xi)}$, A_τ is initially zero. However, since surface tension decreases with temperature, A will increase (decrease) subject to cooling (heating).

4.1.2. *Critical force for pinching*

Using (4.6), the question of whether A can become zero depends on whether G can increase to the value $\sqrt{A_0(\xi)}/\mathscr{F}^*(\xi)$. Examining (4.3), we see that as $\tau \to \infty$, a steady state might be achieved in which either $H(\theta) \to 0$ or $A \to \infty$. The only value of θ for which $H(\theta) = 0$ is $\theta = \theta_h$. Moreover, from (4.6), we see that A must remain bounded if θ is bounded away from θ_h. This implies that the only way that a steady state of (4.3) can be achieved is if $\theta = \theta_h$ and hence $\theta \to \theta_h$ as $\tau \to \infty$. Hence, for a given fluid element, G will increase until the fluid element equilibrates with the heater temperature, that is $\theta = \theta_h$. However, this can only occur if A does not become zero. From (4.6), we hence require $\sqrt{A_0(\xi)} - \mathscr{F}^*(\xi)G(\theta_h, \theta_0(\xi)) > 0$ so that A will always be bounded away from zero. We therefore define the critical force

$$\mathscr{F}_c(\xi) \equiv \frac{\sqrt{A_0(\xi)}}{G(\theta_h, \theta_0(\xi))}, \tag{4.9}$$

below which the cross-section will never become zero at the location ξ. For values of $\mathscr{F}^*(\xi) > \mathscr{F}_c(\xi)$, equations (4.6) and (4.8), if they remain valid, predict that the cross-sectional area A will become zero at a finite time, $\tau_*(\xi)$. When $A = 0$, we can use (4.6) to obtain the value of $\theta = \theta_*(\xi)$ by solving $\sqrt{A_0(\xi)} - \mathscr{F}^*(\xi)G(\theta_*(\xi), \theta_0(\xi)) = 0$. Then $\tau_*(\xi)$ can be obtained by simply substituting $\theta = \theta_*(\xi)$ into (4.8).

It is interesting to note that, if $\mathscr{F}^*(\xi) > \mathscr{F}_c(\xi)$, then $\theta_*(\xi) \neq \theta_h$ and $H(\theta_*(\xi)) \neq 0$. That is, if (4.6) and (4.8) remain valid, the thread does not, in general, equilibrate with the heater. Using (4.3), we also see that $\theta_\tau \to \infty$ as $\tau \to \tau_*(\xi)$. In fact, from (4.1), we see that A_τ tends to a negative constant as $A \to 0$ since $\theta \to \theta_*(\xi)$ and $A \to 0$ as $\tau \to \tau_*(\xi)$. Thus, $A \sim \tau_*(\xi) - \tau$ as $\tau \to \tau_*(\xi)$. Using (4.3), this implies that $\theta - \theta_*(\xi)$ tends to zero like $\sqrt{\tau_*(\xi) - \tau}$.

This phenomenon is based on the assumption that $Re = 0$. For $Re > 0$, equations (4.6) and (4.8) will break down when A becomes sufficiently small (see Wylie *et al.* 2011 for the isothermal case of $0 < Re \ll 1$). When this occurs, the thread will experience the type of surface-tension-driven pinching described by Eggers (1993) and Eggers & Villermaux (2008). For this type of pinching, the radius (rather than the area) tends to zero linearly with τ and so using (4.3) we see that $H(\theta) \to H(\theta_*(\xi)) = 0$ as pinching

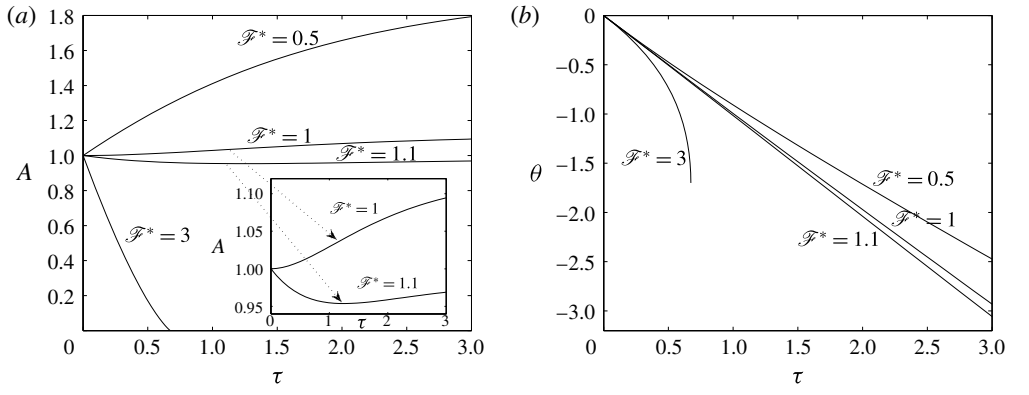

FIGURE 2. Cooling. (*a*) Evolution of cross-sectional area A with different $\mathscr{F}^*$, (*b*) evolution of temperature θ with different $\mathscr{F}^*$. Parameters and conditions: $a = 0.1$, $b = 1$, $H = -1$, $\mathscr{H} = 1$, $\mathscr{F}_c = 2.6692$.

is approached. Therefore, although the $Re = 0$ equations suggest that the thread need not equilibrate with the heater at pinching, for any non-zero Re, the thread must equilibrate to the heater as it pinches.

In summary, for a fixed location ξ, the relation between $\mathscr{F}^*(\xi)$ and $\gamma(\theta_0(\xi))\sqrt{A_0(\xi)}$ determines the initial growth or decay for A, whereas the relation between $\mathscr{F}^*(\xi)$ and $\mathscr{F}_c(\xi)$ determines whether A can ever become zero.

4.1.3. *Numerical examples*

We now illustrate the above conclusions by considering some examples for a fluid element at a location ξ with $\theta_0(\xi) = 0$, $A_0(\xi) = 1$. Here, and for all numerical examples in this paper, we set $\mathscr{H} = 1$. These values of θ_0 and A_0 imply that A will initially increase if $\mathscr{F}^* < 1$ and decrease if $\mathscr{F}^* > 1$. For simplicity, we will consider heating and cooling of the form $H(\theta) = \pm 1$, which corresponds to the case in which the equilibration temperature is assumed to be sufficiently far from the operating temperatures that any changes in temperature do not significantly change the heat flux. Similar results are obtained if one uses the full expression for $H(\theta)$.

Cooling. In figure 2, we show the results for a cooled thread for which the viscosity varies more rapidly with temperature than the surface tension does ($b > a$). The cooling causes both the surface tension and viscosity to increase as time progresses. Using $a = 0.1$ and $b = 1$ and substituting $\theta_h = \infty$ into (4.9) gives $\mathscr{F}_c = 2.6692$. For $\mathscr{F}^* = 3 > \mathscr{F}_c$, A decreases monotonically to zero in a finite time and $\theta_\tau \to -\infty$ as $A \to 0$, as predicted above. For $\mathscr{F}^* < 1$, surface tension always dominates the stretching force in (4.1) and so A monotonically increases. Moreover, as the thread cools, the surface tension increasingly dominates the stretching force and the viscosity increases faster than the surface tension. Therefore, A_τ decreases as time increases. For $\mathscr{F}_c > \mathscr{F}^* = 1.1 > 1$, the stretching force initially dominates and A decreases. However, as the thread cools, the surface tension $\gamma(\theta)$ increases faster than $\sqrt{A}$ decreases in (4.1) and eventually $\gamma(\theta)\sqrt{A} > \mathscr{F}^*$ and thereafter A increases.

Heating. In figure 3, we also consider the case where viscosity varies more rapidly with temperature than the surface tension does ($b > a$), but with heating rather than cooling. The heating causes both the surface tension and viscosity to decrease as

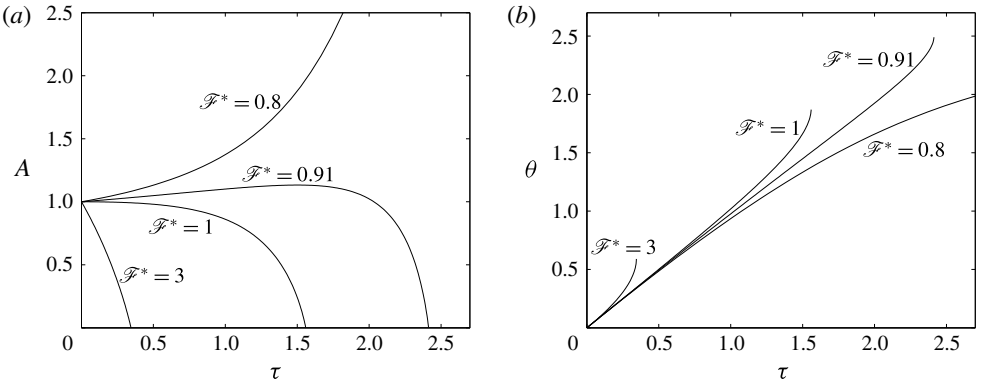

FIGURE 3. Heating. (*a*) Evolution of cross-sectional area A with different $\mathscr{F}^*$, (*b*) evolution of temperature θ with different $\mathscr{F}^*$. Parameters and conditions: $a = 0.1$, $b = 1$, $H = 1$, $\mathscr{H} = 1$, $\mathscr{F}_c = 0.8997$.

time progresses. Using $a = 0.1$ and $b = 1$ and substituting $\theta_h = \infty$ into (4.9) gives $\mathscr{F}_c = 0.8997$. For $\mathscr{F}^* < \mathscr{F}_c = 0.8997$, A will monotonically increase. Moreover, as the thread heats up, the surface tension, $\gamma(\theta)$, decreases more slowly than $\sqrt{A}$ increases in (4.1) and hence $\gamma(\theta)\sqrt{A} - \mathscr{F}^*$ increases with time. In addition, the viscosity decreases with time and hence A_τ increases with time. For $\mathscr{F}^* > 1$, A monotonically decreases until it becomes zero in a finite time. For $1 > \mathscr{F}^* > \mathscr{F}_c$, the surface tension initially dominates and A increases. However, as the thread heats up, the surface tension $\gamma(\theta)$ decreases faster than $\sqrt{A}$ increases in (4.1) and eventually $\gamma(\theta)\sqrt{A} < \mathscr{F}^*$ and thereafter A decreases until it becomes zero in a finite time.

The above study describes the dynamics of a single fluid element. All of the fluid elements evolve independently and so the dynamics appears to be simple, but the collective behaviour can still lead to a number of subtle effects. This is due to the fact that the condition for pinching depends on the evolution of viscosity and surface tension as a function of temperature. Therefore, in order to understand the dynamics of the thread, one needs to consider the dynamics of all of the fluid elements together, as described in the following subsection.

4.2. *Dynamics of stretching of the fluid filament*

The pinching condition for a single fluid element at location ξ is $\mathscr{F}^*(\xi) > \mathscr{F}_c(\xi)$, or alternatively $\mathscr{F} > \mathscr{F}_c(\xi) - Bo \int_\xi^1 A_0(\xi')\,\mathrm{d}\xi'$. Therefore, the critical force for the entire filament is given by $\min_\xi(\mathscr{F}_c(\xi) - Bo \int_\xi^1 A_0(\xi')\,\mathrm{d}\xi')$. For $\mathscr{F} > \min_\xi(\mathscr{F}_c(\xi) - Bo \int_\xi^1 A_0(\xi')\,\mathrm{d}\xi')$, the thread will pinch. In order to find the time at which the thread pinches, one needs to find the fluid element that first achieves $A = 0$, which corresponds to finding $\min_\xi \tau_*(\xi)$. The location of the pinching is then given by finding the value of ξ at which this is achieved, namely $\operatorname{argmin}_\xi \tau_*(\xi)$.

We now consider a set of examples that involve both heating and cooling with a viscosity that varies more rapidly with temperature than surface tension. The basic mechanisms involving thermal effects are broadly similar for both zero and non-zero Bo threads. Therefore, we mostly focus on results for $Bo = 0$ in this paper. However, we give two examples with $Bo \neq 0$ (figures 13 and 14) in the final examples at the end of § 5.

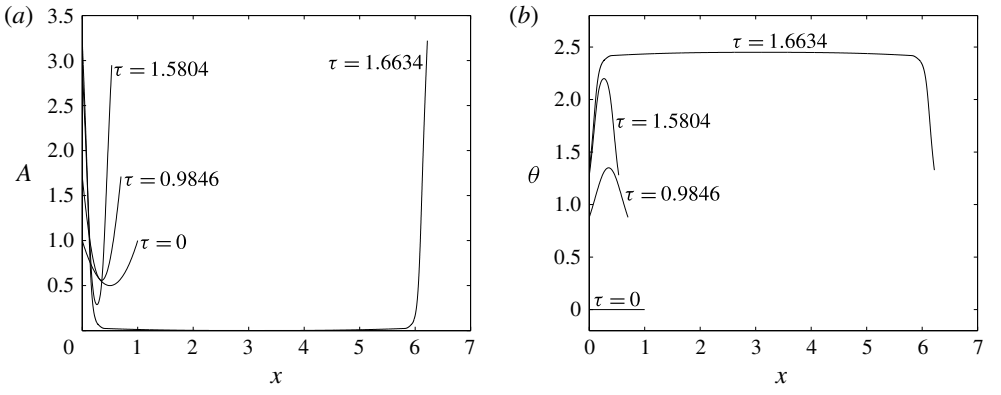

FIGURE 4. Results in Eulerian coordinates for heating with $\theta_0(\xi) = 1$ and where $A_0(\xi)$ has a minimum point. (*a*) Evolution of cross-sectional area A, (*b*) evolution of temperature θ. Parameters and conditions used: $a = 0.1$, $b = 1$, $H = 1$, $\mathscr{H} = 1$, $A_0(\xi) = 0.5 + 2(\xi - 0.5)^2$, $\theta_0(\xi) = 0$, $\mathscr{F} = 0.645 > \mathscr{F}_c(\xi = 0.5)$, $Bo = 0$.

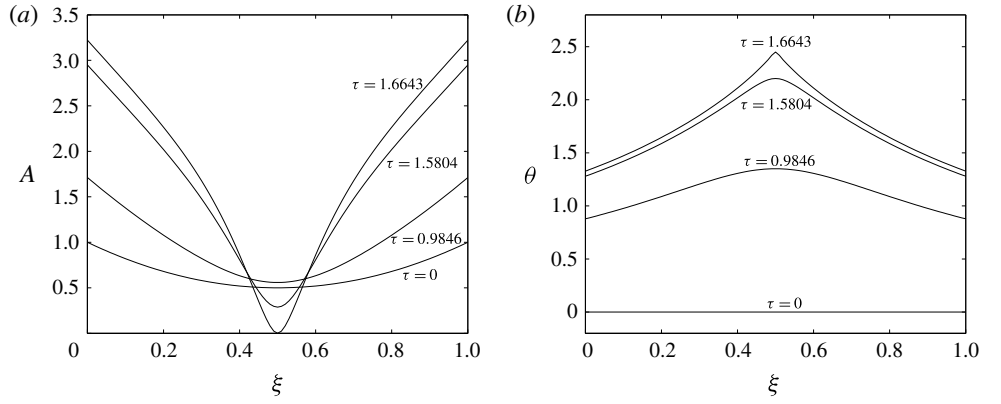

FIGURE 5. Results in Lagrangian coordinates for heating with $\theta_0(\xi) = 1$ and where $A_0(\xi)$ has a minimum point. (*a*) Evolution of cross-sectional area A, (*b*) evolution of temperature θ. Parameters and conditions used: $a = 0.1$, $b = 1$, $H = 1$, $\mathscr{H} = 1$, $A_0(\xi) = 0.5 + 2(\xi - 0.5)^2$, $\theta_0(\xi) = 0$, $\mathscr{F} = 0.645 > \mathscr{F}_c(\xi = 0.5)$, $Bo = 0$. Note that the evolution of A near $\xi = 0.5$ is non-monotonic.

4.2.1. *Uniform heating*

We first consider the case of uniform heating with two different initial conditions. In figures 4 and 5, we show results for an example with uniform heating in which the initial temperature is zero and the initial cross-section has a minimum at its midpoint. Figure 4 shows the results in Eulerian coordinates while figure 5 shows the results in Lagrangian coordinates. As one can see from figure 4, it is very hard to visualize the early time evolution clearly in Eulerian coordinates since the thread is dramatically stretched as pinching is approached. Therefore, in the rest part of the paper, we present all the results in Lagrangian coordinates except for the example (figure 12) in which spatially non-uniform heating is applied.

From figure 5, one can easily find that the cross-section of all of the fluid elements initially increases due to the small extensional force. However, the thread is thinner

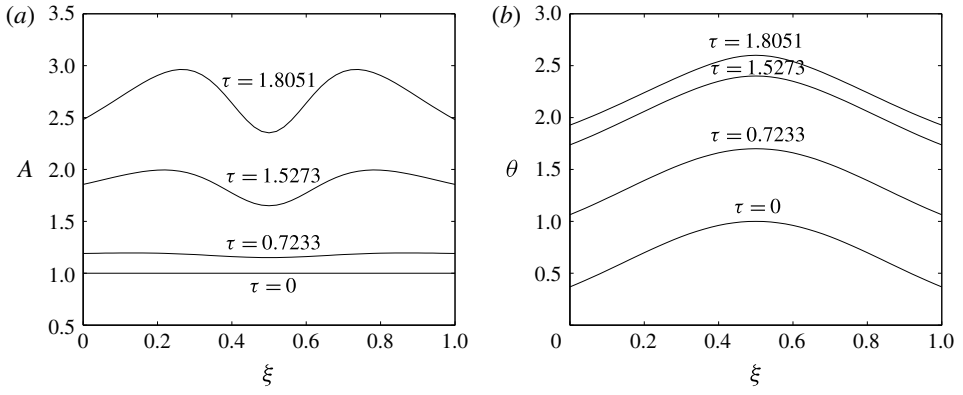

FIGURE 6. Results for heating when $\theta_0(\xi)$ has a local maximum and $A_0(\xi) = 1$. (*a*) Evolution of cross-sectional area A, (*b*) evolution of temperature θ. Parameters and conditions used: $a = 0.1$, $b = 1$, $H = 1$, $\mathscr{H} = 1$, $A_0(\xi) = 1$, $\theta_0(\xi) = \exp(-(\xi - 0.5)^2)$, $\mathscr{F} = 0.84 < \mathscr{F}_c(\xi = 0.5)$, $Bo = 0$.

in the middle and the fluid elements located there heat up more rapidly than the fluid elements near the two ends. This leads to the surface tension coefficient for the fluid elements near the middle to eventually become sufficiently small that the stretching force dominates and the thread eventually pinches in the middle. The fluid elements near the ends, by contrast, cannot heat up sufficiently for the pulling force to overcome the surface tension and they therefore increase monotonically.

As our second example, we show the results in figure 6 for uniform heating in which the initial cross-section is uniform and the initial temperature has a maximum at its midpoint. In this case, the stretching force is sufficiently small that the cross-section of all fluid elements increases indefinitely. Perhaps surprisingly, the largest cross-section is neither found at the middle nor the ends of the thread. By examining (4.1), we see that this occurs as the result of two competing mechanisms. As the fluid elements heat up, the viscosity decreases more rapidly than the surface tension. On the one hand, if $\gamma(\theta)\sqrt{A}$ is sufficiently large compared with $\mathscr{F}$, then the dominant effect of higher temperatures on the right-hand side of (4.1) will be to decrease the viscosity and hence the hotter elements will grow faster than the cooler elements. This explains why the fluid elements at the ends grow more slowly than their neighbours. On the other hand, if $\gamma(\theta)\sqrt{A}$ is only slightly larger than $\mathscr{F}$, then the dominant effect of higher temperatures will be to reduce the numerator in the right-hand side of (4.1) and hence the hotter elements will grow more slowly than the cooler elements. This explains why the fluid elements in the middle grow more slowly than their neighbours. These two effects combine to generate the two local maxima observed in figure 6.

4.2.2. *Uniform cooling*

In figure 7, we show results for an example with uniform cooling in which the initial cross-section is uniform and the initial temperature has a maximum at its midpoint. In this case, the stretching force is sufficiently large that all fluid elements will monotonically thin with time. The hottest fluid elements that are initially near the middle have smaller surface tension than the fluid elements near the ends. This means that they are more strongly affected by the stretching force and hence thin more rapidly. Since these elements have thinner cross-section, they are more rapidly

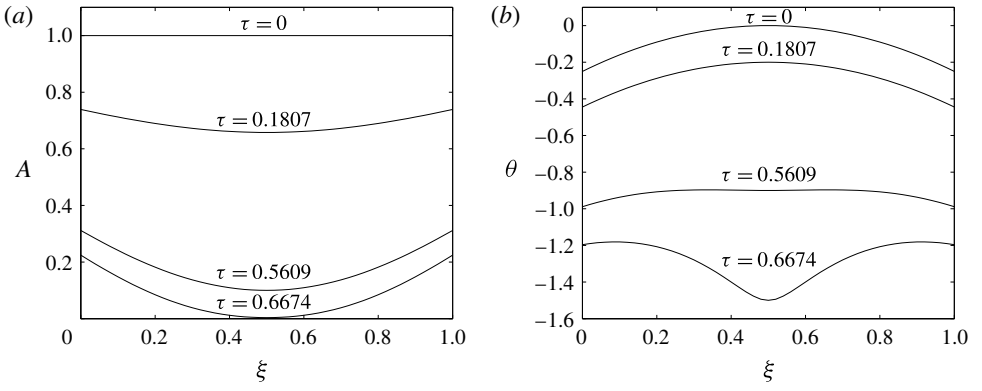

FIGURE 7. Results for cooling when $\theta_0(\xi)$ has a local maximum and $A_0(\xi) = 1$. (*a*) Evolution of cross-sectional area A, (*b*) evolution of temperature θ. Parameters and conditions used: $a = 0.1$, $b = 1$, $H = -1$, $\mathscr{H} = 1$, $A_0(\xi) = 1$, $\theta_0(\xi) = -(\xi - 0.5)^2$, $\mathscr{F} = 3 > \mathscr{F}_c(\xi = 0.5)$, $Bo = 0$.

affected by the external cooling than the fluid elements that were initially cooler. When pinching occurs, the fluid elements in the middle become the coolest in the entire thread as observed in figure 7.

5. Inertial effects

When $Re = 0$ and $H = H(\theta)$, all the fluid elements evolve independently and satisfy (4.1) and (4.3). However, when $Re \neq 0$, this is no longer true. The effects of inertia can be most readily understood by considering the integral of (3.7) with respect to ξ. After applying the boundary condition of fixed extensional force at the free end point $\xi = 1$, we obtain

$$\mathscr{F} + Bo \int_{\xi}^{1} A_0(\xi')\,\mathrm{d}\xi' - Re\frac{\partial}{\partial\tau}\left[\int_{\xi}^{1} A_0(\xi')u(\xi',\tau)\,\mathrm{d}\xi'\right] = -\mu(\theta)A_\tau + \gamma(\theta)\sqrt{A}. \quad (5.1)$$

If $Re = 0$, the effective stretching force on the left-hand side of (5.1) is the function $\mathscr{F}^*(\xi)$. This corresponds to the stretching force imposed at the free end point being perfectly transmitted throughout the length of the thread. If $Re \neq 0$, then the effective stretching force will be modified by the integral on the left-hand side of (5.1). For $Re \ll 1$, this effective force modification will be small and the motion will be well approximated by the $Re = 0$ solution unless the extension of the thread becomes sufficiently large that the acceleration $\partial u/\partial\tau$ becomes of $O(Re^{-1})$, which corresponds to A becoming small. When this occurs, the stretching force will not be transmitted effectively through the regions of small A and the stretching will be reduced.

We now show the results of numerical simulations that illustrate the phenomena that can occur when inertia is included. In order to solve (3.6)–(3.9) numerically, we spatially discretized (3.6)–(3.8) using second-order central differences. We then solved the resulting system of ordinary differential equations with a standard numerical solver. At each time step, we integrated (3.9) using a trapezoid rule to obtain the relation between the Lagrangian and Eulerian coordinates. We note that if the heater is spatially uniform, then (3.9) decouples from (3.6)–(3.8). The grid points are uniformly distributed in the Lagrangian coordinate and so if the thread becomes highly extended

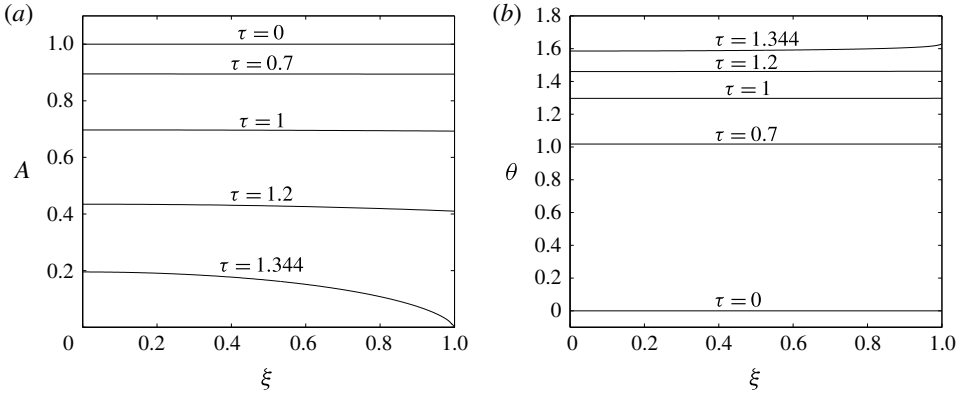

FIGURE 8. Numerical results for a thread with initially uniform radius and temperature subjected to spatially uniform heating. (*a*) Evolution of A. (*b*) Evolution of θ. Parameters and conditions used: $a = 0.1$, $b = 1$, $A_0(\xi) = 1$, $\theta_0(\xi) = 0$, $\mathscr{F} = 1.0005$, $Re = 0.001$, $H = 2 - \theta$, $\mathscr{H} = 1$, $Bo = 0$.

in some regions, then the distance between neighbouring grid points in Eulerian space will become large. This phenomena has been shown to lead to numerical inaccuracies (Stokes & Tuck 2004) when dealing with the Lagrangian equations. In order to prevent this, if the grid spacing exceeded a threshold, we used linear interpolation to add additional grid points in the affected regions.

5.1. *Thinning under spatially uniform conditions*

We begin by considering the case in which $A_0(\xi) = 1$ and $\theta_0(\xi) = 0$ with a spatially uniform heater and an extensional force larger than the critical value. If inertia is completely neglected, then all fluid elements will behave in an identical way and the thread will thin in a spatially uniform way. For $Re = 0.001$ used in figure 8, the early evolution is well approximated by spatially uniform thinning. However, when the thread thins sufficiently, inertial effects reduce the effective stretching force as one moves away from the pulled end. This implies that the rate of thinning will be largest at the pulled end and so A will first become zero at the free end of the thread. This is seen to occur in the later stages of stretching in figure 8.

5.2. *Thinning under non-uniform initial temperature*

In this subsection, we will use a set of examples to illustrate that the pinching location for a preheated thread with non-zero Reynolds number is determined by three different mechanisms: extensional force-driven pinching, surface-tension-driven pinching and largest-temperature-gradient-driven pinching.

Extensional force-driven pinching versus surface-tension-driven pinching. We consider a case with an initially uniform cross-section, $A_0(\xi) = 1$, a spatially uniform heater, a stretching force greater than the critical value and an initial temperature profile with the maximum at the upper boundary of the thread. For a small $Re = 0.01$ (figure 9*a*), the motion is very similar to the $Re = 0$ behaviour until the thread becomes thin, the thread then undergoes surface-tension-driven pinching at the upper boundary of the

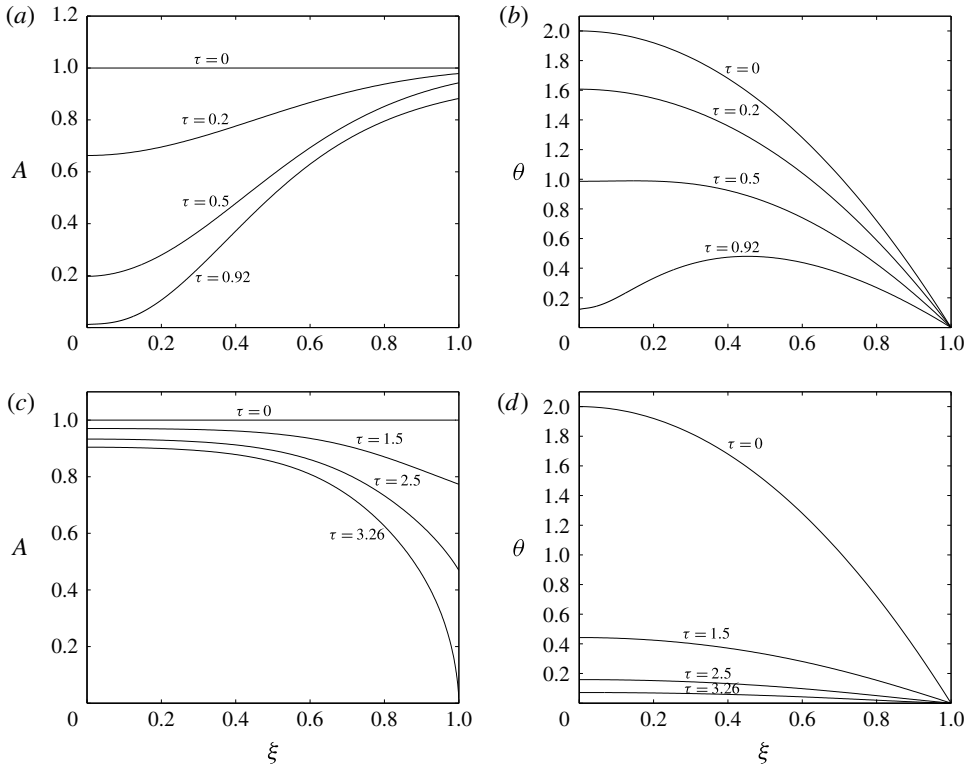

FIGURE 9. Numerical results for a uniform thread whose initial temperature $\theta_0(\xi)$ is maximum at the upper boundary point $\xi = 0$. (*a*,*b*) $Re = 0.01$ (small Re), pinching happens at the hottest point, i.e. $\xi = 0$. (*c*,*d*) $Re = 10$ (relatively large Re), pinching happens at the pulled end. Parameters and conditions used: $a = 0.1$, $b = 1$, $A_0(\xi) = 1$, $\theta_0(\xi) = 2(1 - \xi^2)$, $\mathscr{F} = 1.1$, $H(\theta) = -\theta$, $\mathscr{H} = 1$, $Bo = 0$.

thread. However, for a larger $Re = 10$, the situation is different (figure 9*c*). The inertial effects are significant even in the early stages of pulling and this means that the stretching force is far from being uniformly transmitted through the length of the thread. This implies that stretching is much more significant near the pulled end of the thread and this causes the cross-sectional area to become zero at the pulled end. Hence, for small Re the thread will pinch at the hottest point, whereas for larger Re the thread will pinch at the pulled end.

Extensional force-driven pinching versus largest-temperature-gradient-driven pinching. In this case, we will show that another mechanism can also affect the place where the pinching occurs. Again, we consider an initially uniform cross-section, $A_0(\xi) = 1$, a spatially uniform heater and a stretching force greater than the critical value. However, in this case, we adopt an initial temperature profile that is uniformly hot near the upper boundary of the thread and uniformly cool near the pulled end. The two constant regions are joined together by a thin transition region. For a relatively large $Re = 20$ (figure 10*c*), the behaviour is similar to that shown in the previous example, with significant thinning near the pulled end of the thread until the cross-sectional area becomes zero there. However, for a relatively small $Re = 1$

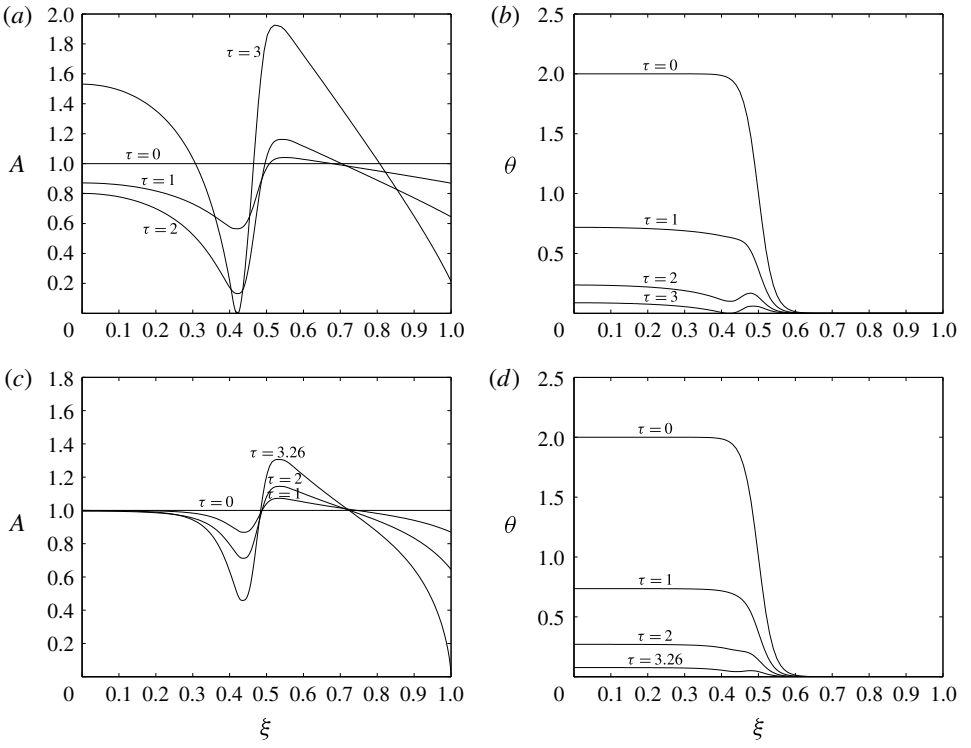

FIGURE 10. Numerical results for a thread whose initial temperature $\theta_0(\xi)$ is two different constants near the two end points and has a rapid transition near $\xi = 0.5$. (*a*,*b*) $Re = 1$ (relatively small Re), pinching happens at the fluid element that initially had a large temperature gradient, i.e. $\xi = 0.5$. (*c*,*d*) $Re = 20$ (relatively large Re), pinching happens at the pulled end. Parameters and conditions used: $a = 0.1$, $b = 1$, $A_0(\xi) = 1$, $\theta_0(\xi) = 2(1 + \tanh((0.5 - \xi)/\epsilon))$, $\epsilon = 0.04$, $\mathscr{F} = 1.1$, $H(\theta) = -\theta$, $\mathscr{H} = 1$, $Bo = 0$.

(figure 10*a*), the behaviour is quite different. Using (3.6), we can rewrite (3.7) for $Bo = 0$ in the form

$$Reu_\tau = \frac{1}{A_0}\left(\mu(\theta)\frac{A^2}{A_0}u_\xi + \gamma(\theta)\sqrt{A}\right)_\xi. \tag{5.2}$$

Since we chose initial conditions $u(\xi, 0) = 0$ and $A(\xi, 0) = 1$, we see that during the very early stages of the dynamics, the right-hand side of (5.2) is dominated by the surface tension force term $(\gamma(\theta)\sqrt{A})_\xi$. For the temperature profile we have chosen, the surface tension will be small and constant near the upper boundary of the thread, large and constant near the pulled end of the thread and have a large slope in the thin transition region. This gradient in the surface tension will initially cause an acceleration of the fluid elements in the transition region towards the pulled end of the thread. Since mass must be conserved, this acceleration causes thinning of the fluid elements on the hot side of the transition region and broadening of the fluid elements on the cool side of the region. Therefore, during the initial stages, there is a local minimum in the cross-section on the hot side of the transition region and a local maximum on the cool side. The thread then is stretched by the imposed force

until a fluid element on the hot side of the transition region experiences pinching. We note that if the initial temperature profile had been such that the thread was cooler near the upper boundary and hotter near the pulled end, then the surface tension would have been initially large near the upper boundary and small near the pulled end. This would induce accelerations in the transition regions away from the pulled end. Therefore, we would also observe pinching in the fluid elements on the hot side of the transition region.

Extensional force-driven pinching versus largest-temperature-gradient-driven pinching versus surface-tension-driven pinching. On the one hand, figure 9 illustrated how pinching can occur in the hottest region for a small Re and at the pulled end for a larger Re. On the other hand, figure 10 illustrated how pinching can occur near the large temperature gradients for a relatively small Re and at the pulled end for a relatively large Re. Therefore, there are three possible mechanisms: at a relatively large Re, the force transmission is weak and the thread will tend to pinch at the pulled end; for a relatively small Re the hottest part of the thread will have the lowest viscosity and weakest surface tension and so will tend to pinch there; and for an intermediate Re, if there are large gradients in temperature, accelerations can be induced that lead to pinching in fluid elements near the large gradients.

We now consider an example that includes a competition between all three of the mechanisms illustrated in the previous two examples. To do this, we take an initial temperature profile with a maximum at the upper boundary of the thread but with a sharp transition to lower temperatures (see the initial temperature function $\theta_0(\xi)$ in figure 11*b*). For a small $Re = 0.01$, the acceleration induced near the sharp transition is sufficiently small that the minimum cross-section is always located at the upper boundary (at the hottest point) and the thread ultimately pinches there (figure 11*a*). We note that at early times, the cross-sectional area of all of the fluid elements decreases with time. In fact, during early times, A is well approximated by the inertialess evolution equation (4.1) and there are no significant accelerations induced by the temperature gradients. This is because Re is small and $A = O(1)$. However, at later times, when A becomes smaller, accelerations do become significant and cause the thread to thin on the hot side of the transition and thicken on the cool side of the transition, but the effect is too weak to cause pinching to occur on the hot side of the transition. For an intermediate $Re = 1$, the acceleration induced by the surface tension gradient is large enough that the minimum cross-section occurs near the transition and the thread therefore pinches near the transition region (figure 11*c*). Finally, for a relatively large $Re = 20$, the transmission of the stretching force is sufficiently weak that the thread pinches at the pulled end (figure 11*e*). We have therefore shown that the location at which pinching occurs is quite subtly affected by Re.

5.3. *Thinning under non-uniform heating*

In this subsection, we present results for the case of a non-uniform heater in figure 12. We will use an example to illustrate that the competition seen in the above examples can also occur in this case. We consider initial conditions that are spatially uniform, $A_0(\xi) = 1$ and $\theta_0(\xi) = 0$ with an extensional force larger than the critical value. We choose a heater profile that has a high heating rate in a finite region near the upper boundary of the thread with a local maximum at the upper boundary and a rapid transition to a lower heating rate outside of the finite region, see figure 12. In some ways, the dynamics is very similar to the preheated case, but there is an

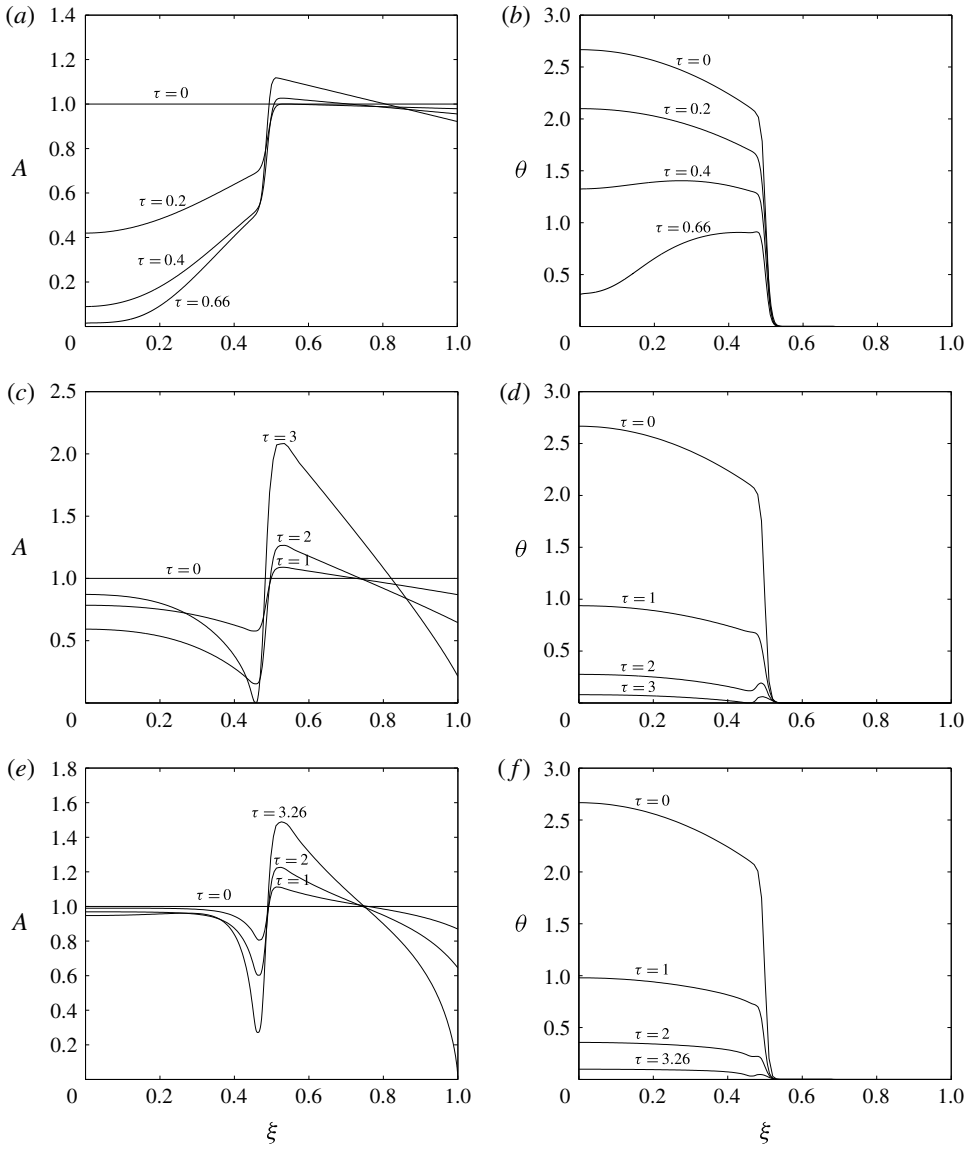

FIGURE 11. Numerical results for a thread whose initial temperature $\theta_0(\xi)$ is maximum at the upper boundary point $\xi = 0$ and has a rapid transition down to zero near $\xi = 0.5$. (*a*,*b*) $Re = 0.01$ (small *Re*), pinching happens at the hottest point, i.e. $\xi = 0$. (*c*,*d*) $Re = 1$ (intermediate *Re*), pinching happens for a fluid element that was initially near the large temperature gradient, i.e. $\xi = 0.5$. (*e*,*f*) $Re = 20$ (relatively large *Re*), pinching happens at the pulled end. Parameters and conditions used: $a = 0.1$, $b = 1$, $A_0(\xi) = 1$, $\theta_0(\xi) = 8/3(1-\xi^2)(1+\tanh((0.5-\xi)/\epsilon))/2$, $\epsilon = 0.01$, $\mathscr{F} = 1.1$, $H(\theta) = -\theta$, $\mathscr{H} = 1$, $Bo = 0$.

important difference. Fluid elements that start in the region with large heating rate heat up and experience lower surface tension and have lower viscosities and hence thin more rapidly than fluid elements that start in the region with lower heating rate. However, this thinning causes the fluid elements to extend and hence move out of the

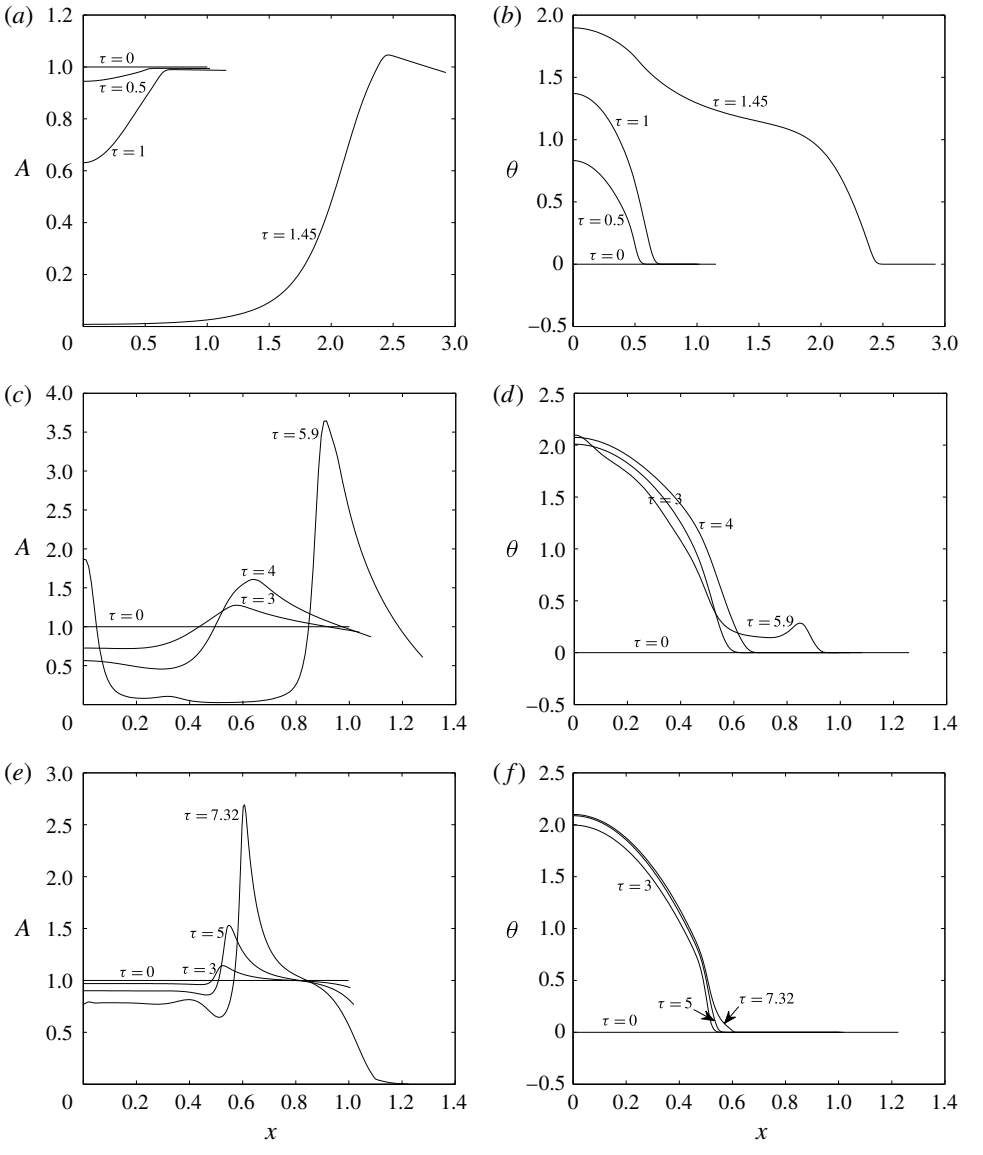

FIGURE 12. Numerical results for a thread with initially uniform radius and uniform temperature but with spatially non-uniform heating, where the external heater temperature θ_h is maximum at the upper boundary $x=0$ and has a rapid transition to zero near $x=0.5$. (*a*,*b*) $Re=0.01$ (small Re), pinching happens at the hottest point, i.e. $x=0$. (*c*,*d*) $Re=10$ (moderately large Re), pinching happens for a fluid element that was initially near the large temperature gradient $x=0.5$. (*e*,*f*) $Re=100$ (large Re), pinching happens at the pulled end. Parameters and conditions used: $a=0.1$, $b=1$, $A_0(\xi)=1$, $\theta_0(\xi)=0$, $\mathscr{F}=1.05$, $H(\theta)=1.05(1-3x^2)(1+\tanh((0.5-x)/\epsilon))-\theta$, $\epsilon=0.04$, $\mathscr{H}=1$, $Bo=0$.

region with large heating rate. Only the fluid elements very close to the centreline experience strong heating for extended lengths of times. This results in a smoothing effect on the temperature profiles in the thread and tends to reduce the magnitude

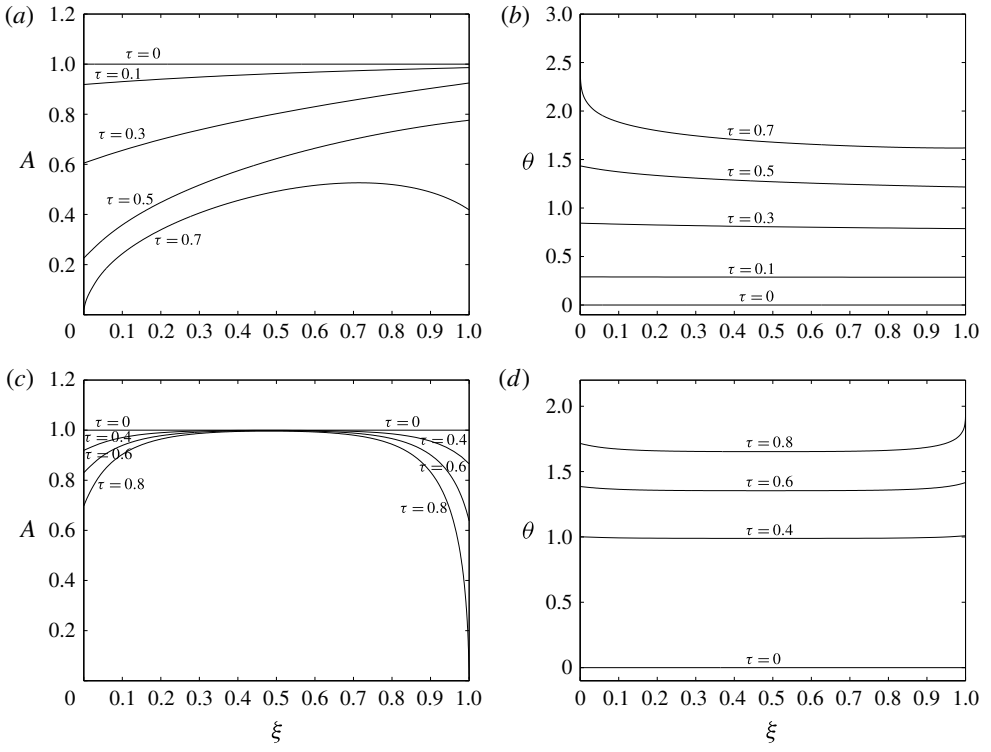

FIGURE 13. Numerical results for a thread falling under gravity with non-zero stretching force and initially uniform temperature. (*a*,*b*) $Re = 0.1$ (small Re), pinching occurs at the top, i.e. $\xi = 0$. (*c*,*d*) $Re = 10$ (relatively large Re), pinching occurs at the pulled end, i.e. $\xi = 1$. Parameters and conditions used: $a = 0.1$, $b = 1$, $A_0(\xi) = 1$, $\theta_0(\xi) = 0$, $\mathscr{F} = 1.1$, $H(\theta) = 3 - \theta$, $\mathscr{H} = 1$, $Bo = 1$.

of the mechanism associated with temperature gradients that caused pinching in the preheated case. If the heating rate does not have an especially large spatial gradient, then small Re solutions will pinch at the upper boundary and large Re solutions will pinch at the pulled end point. Nevertheless, if we choose the transition zone in the heating rate to be sufficiently narrow, the surface-tension-gradient effect will cause pinching to occur to fluid elements that started near the edge of the transition zone, see figure 12.

5.4. *Thinning with non-zero gravity*

Finally, in this subsection, we consider two examples with non-zero Bo as shown in figures 13 and 14. Figure 13 shows the case in which the thread is falling under gravity with a non-zero stretching force. The thread has initially uniform temperature and radius and is subjected to spatially uniform external heating from the environment. The stretching force applied at the pulled end is chosen to be greater than the critical value so that pinching would occur at the free end in the absence of gravity. The results are qualitatively similar to the $Bo = 0$ case in the sense that, depending on Re, pinching can happen either at the top or at the pulled end. For $Re = 0$, the dynamics of the cross-sectional area is determined by (4.1) and (4.2) and the maximum extensional

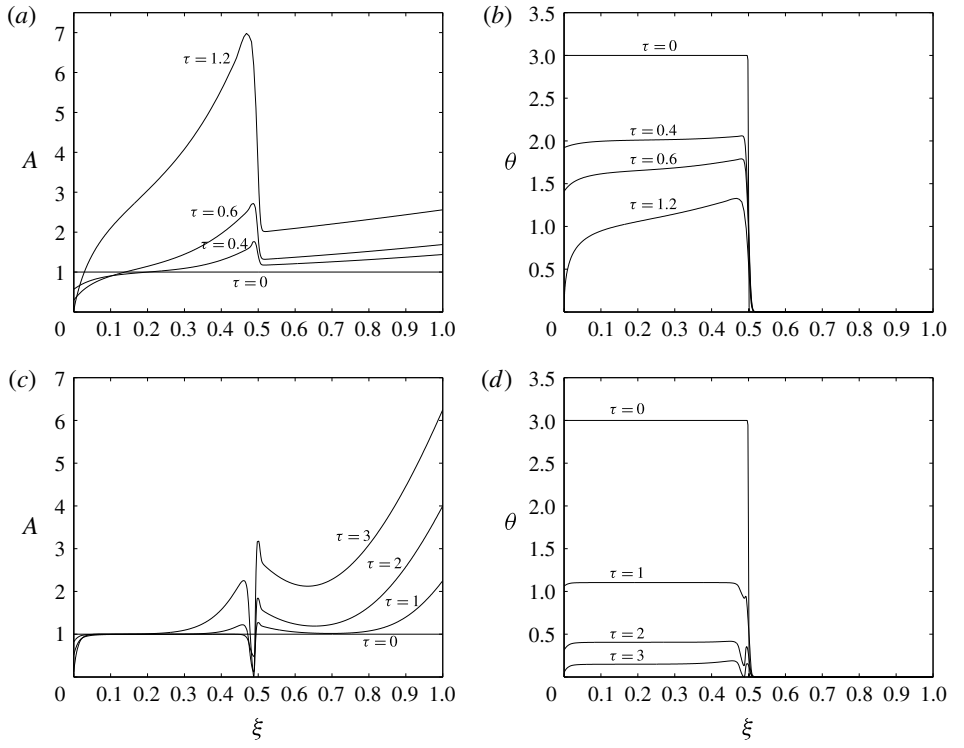

FIGURE 14. Numerical results for a thread falling under gravity with zero stretching force and non-uniform initial temperature, where the initial temperature $\theta_0(\xi)$ has a rapid transition near $\xi = 0.5$. (*a*,*b*) $Re = 1$ (small Re), pinching happens at the top end due to the weight of the thread. (*c*,*d*) $Re = 100$ (large Re), pinching occurs at a fluid element that was initially near the large temperature gradient. Parameters and conditions used: $a = 0.1$, $b = 1$, $A_0(\xi) = 1$, $\theta_0(\xi) = 3(1 + \tanh((0.5 - \xi)/\epsilon))/2$, $\epsilon = 0.005$, $\mathscr{F} = 0$, $H(\theta) = -\theta$, $\mathscr{H} = 1$, $Bo = 0.5$.

force occurs at the top of the thread where the supported weight is maximal. This means that an initially uniform thread with uniform heating will always pinch at the top. For sufficiently small Re, inertia plays a small role and pinching is observed to occur at the top (figure 13*a*). For larger Re, the force applied at the end of the thread is not uniformly transmitted through the thread. Inertia also acts to reduce the effective stretching force due to gravity. This means that the stretching force at the top will be reduced by inertia. At the free end of the thread, the force is fixed and so inertia has no effect. Therefore, for sufficiently large Re, we expect that pinching will happen at the pulled end. This is observed for $Re = 10$ in figure 13(*c*).

In figure 14, we consider a case with initially uniform radius and uniform environment, but an initial temperature profile with a sharp transition. However, rather than using a non-zero extensional force at the pulled end with zero gravity (as we used in figures 8–11), we use zero extensional force $\mathscr{F} = 0$ and non-zero gravity $Bo \neq 0$. Since $\mathscr{F} = 0$, the effective stretching force at the free end is zero so that pinching cannot happen at the pulled end. Therefore, there are only two mechanisms that can lead to pinching rather than three mechanisms seen in figure 11. Pinching can happen due to the weight of the thread at low Re (figure 14*a*) or due to the flow induced by temperature variations at high Re (figure 14*c*).

6. Conclusions

In this paper, we have studied a model of a long and thin viscous thread for which both viscosity and surface tension depend on temperature. Our methodology allows us to study threads that are extending by falling under their own weight, by being pulled by an external force applied at the end point or by a combination of both of these two. By adopting a Lagrangian framework, we have obtained analytical solutions for zero Reynolds number solutions with uniform external heating. Our results are valid for arbitrary initial cross-sectional area and temperature profiles. We have derived the criterion that determines whether a thread will exhibit surface-tension-driven pinching. Moreover, we have shown that these solutions show a surprisingly rich set of dynamics. In particular, for heated threads, the cross-sectional area can thicken at early times and then thin and ultimately pinch. In contrast, for cooled threads, the cross-sectional area can thin at early times and then thicken at later times. We have also derived expressions for the parameter ranges in which this non-monotonic behaviour occurs. The solutions also exhibit non-monotonic behaviour in space. In the case of heating, a thread with initially uniform cross-section and an initial local minimum in the temperature profile can develop two local maxima and a local minimum in the cross-section. For similar initial conditions in the case of cooling, the temperature profile can evolve from having an initial local maximum to having two local maxima separated by a local minimum.

We have also obtained numerical solutions for the case in which inertial effects are included. Results show that inertia can play multiple roles in the dynamics and that the location at which pinching occurs can be subtly affected by inertia. In particular, for sufficiently low Reynolds number, the location of the pinching (if it occurs at all) will happen at a location close to the pinching location for the zero Reynolds number case. For sufficiently large Reynolds number, if there is a non-zero pulling force applied to the end of the thread, the thread can pinch at the end at which the force is applied. This is due to the fact that inertia reduces the effective pulling force that is transmitted through the thread and hence reduces the effective stretching in the bulk of the thread. However, if there is zero pulling force applied to the end of the thread and the thread thins purely due to falling under its own weight, pinching will never occur at the free end no matter how large the Reynolds number. Finally, for intermediate Reynolds numbers, if there is a sufficiently abrupt change in the initial temperature it can induce accelerations of the fluid elements in the region in which temperature changes occur. This can lead to a local maximum and minimum to develop in the cross-section that ultimately can lead to pinching that occurs at the fluid elements that were initially located near the abrupt temperature change.

Therefore, in the case of a thread with a non-zero pulling force applied to the end of the thread, there are three separate mechanisms that can lead to very different kinds of pinching for different values of the Reynolds number. And in the case of a thread with a zero pulling force applied to the end of the thread, there are only two mechanisms that can occur. The case of non-uniform external heating has very similar mechanisms. These results have important consequences when determining the appropriate operating conditions under which the extension of fibres can be undertaken so that surface-tension-driven pinching does not occur. This is clearly of major importance in applications. We also note that inertia tends to decrease the force transmission through the thread so that zero Reynolds number solutions give a useful lower bound on the applied force for pinching to occur.

In the paper, we have focused on the case in which heat loss and gain is governed by Newton's heat transfer law. For more complicated heat transfer models that may

include the effects of radiative and convective heating and cooling from the surface, the analysis in this paper carries over directly. The only difference will be in the function $H(x, \theta)$ that characterises the heat transport.

We point out that the methodology used in this paper can be easily extended to the case of an axisymmetric hollow tube. Using similar techniques to those used in this paper, we can derive the long-wavelength equations for the cross-sectional area of the tube, the ratio of inner and outer radius, the axial velocity and the temperature. If we neglect the inertial term, we can also obtain some analytical results similar to those in this paper. Furthermore, one can then readily show that the ratio of inner and outer radius is always decreasing. We omit the detailed derivation and analysis here. We note that the above results obtained for tubes represent an extension of the results in Huang *et al.* (2007), who neglected surface tension effects.

Finally, we mention that the problem with constant surface tension has been studied for a general non-axisymmetric thread with an arbitrary number of holes by Stokes *et al.* (2014). Using a similar approach to Cummings & Howell (1999), they showed that the cross-plane flow decouples from the axial flow and the solution can be found in a particularly convenient way. For a non-axisymmetric thread with temperature-dependent surface tension and viscosity, one can use a similar approach to show that the cross-plane flow evolves independently of the axial flow. One can hence obtain a model for the cross-sectional area, axial velocity and temperature similar to (3.6)–(3.8), where the surface tension term in the momentum equation will involve the total boundary length from the cross-plane problem (see Stokes *et al.* 2014). Therefore, the problem for non-axisymmetric threads with temperature-dependent surface tension and viscosity can also be solved in a convenient way.

Acknowledgements

D.H. was supported by the Natural Science Foundation of China (no. 11402174), the Fundamental Research Funds for the Central Universities, the Program for Young Excellent Talents at Tongji University (no. 2013KJ012) and the Scientific Research Foundation for the Returned Overseas Chinese Scholars, State Education Ministry. J.J.W. was supported by the Research Grants Council of Hong Kong (grant no. CityU 103313), H.H. by NSERC, and R.M.M. by NSF.

REFERENCES

ARGYROS, A. 2013 Microstructures in polymer fibres for optical fibres, THz waveguides, and fibre-based metamaterials. *ISRN Optics* 785162.

ASHBY, M. & JONES, R. H. D. 2013 *Engineering Materials 2: An Introduction to Microstructures and Processing*, 4th edn, pp. 393–473. Butterworth-Heinemann.

BANSAL, N. P. & DOREMUS, R. H. 1986 *Handbook of Glass Properties. Materials Engineering Department Rensselaer Polytechnic Institute Troy*. Academic.

BINGHAM, P. A. 2010 Design of new energy-friendly compositions. In *Fiberglass and Glass Technology: Energy-Friendly Compositions and Applications* (ed. F. T. Wallenberger & P. A. Bingham), pp. 267–351. Springer.

BLYTH, M. G. & BASSOM, A. P. 2012 Flow of a liquid layer over heated topography. *Proc. R. Soc. Lond.* A **468**, 4067–4087.

BRADSHAW-HAJEK, B. H., STOKES, Y. M. & TUCK, E. O. 2007 Computation of extensional fall of slender viscous drops by a one-dimensional Eulerian method. *SIAM J. Appl. Maths* **67**, 1166–1182.

CHEN, J. C., SHEU, J. C. & LEE, Y. T. 1990 Maximum stable length of nonisothermal liquid bridges. *Phys. Fluids* **2**, 1118–1123.

CHEN, Y. J., ABBASCHIAN, R. & STEEN, P. H. 2003 Thermocapillary suppression of the Plateau–Rayleigh instability: a model for long encapsulated liquid zones. *J. Fluid Mech.* **485**, 97–113.

CHINNOV, E. A. & SHATSKIY, E. N. 2014 Thermocapillary instabilities in a falling liquid film at small Reynolds numbers. *Tech. Phys. Lett.* **40**, 7–9.

CRASTER, R. V. & MATAR, O. K. 2009 Dynamics and stability of thin liquid films. *Rev. Mod. Phys.* **81**, 1131–1198.

CUMMINGS, L. J. & HOWELL, P. D. 1999 On the evolution of non-axisymmetric viscous fibres with surface tension, inertia and gravity. *J. Fluid Mech.* **389**, 361–389.

D'ALESSIO, S. J. D., PASCAL, J. P. & JASMINE, H. A. 2010 Film flow over heated wavy inclined surfaces. *J. Fluid Mech.* **665**, 418–456.

DENN, M. M. 1980 Continuous drawing of liquids to form fibers. *Annu. Rev. Fluid Mech.* **12**, 365–387.

DENN, M. M. 2014 *Polymer Melt Processing: Foundations in Fluid Mechanics and Heat Transfer. (Part of Cambridge Series in Chemical Engineering)*. Cambridge University Press.

DEWYNNE, J. N., HOWELL, P. D. & WILMOTT, P. 1994 Slender viscous fibers with inertia and gravity. *Q. J. Mech. Appl. Maths* **47**, 541–555.

DEWYNNE, J. N., OCKENDON, J. R. & WILMOTT, P. 1992 A systematic derivation of the leading-order equations for extensional flows in slender geometries. *J. Fluid Mech.* **244**, 323–338.

DIJKSTRA, H. A. & STEEN, P. H. 1991 Thermocapillary stabilization of the capillary break up of an annular film of fluid. *J. Fluid Mech.* **229**, 205–228.

EGGERS, J. 1993 Universal pinching of 3D axisymmetric free-surface flow. *Phys. Rev. Lett.* **71**, 3458–3460.

EGGERS, J. & VILLERMAUX, E. 2008 Physics of liquid jets. *Rep. Prog. Phys.* **71**, 036601.

FITT, A. D., FURUSAWA, K., MONRO, T. M. & PLEASE, C. P. 2001 Modeling the fabrication of hollow fibers: capillary drawing. *J. Lightwave Technol.* **19**, 1924–1931.

FLUEGEL, A. 2007 Glass viscosity calculation based on a global statistical modeling approach. *Glass Technol.: Eur. J. Glass Sci. Technol.* **48**, 13–30.

FOREST, M. G. & ZHOU, H. 2001 Unsteady analysis of thermal glass fiber drawing processes. *Eur. J. Appl. Maths* **12**, 479–496.

GALLACCHI, R., KÖLSCH, S., KNEPPE, H. & MEIXNER, A. J. 2001 Well-shaped fibre tips by pulling with a foil heater. *J. Microsc.* **202**, 182–187.

GOSPODINOV, P. & YARIN, A. L. 1997 Draw resonance of optical microcapillaries in non-isothermal drawing. *Intl J. Multiphase Flow* **23**, 967–976.

GOUSSIS, D. A. & KELLY, R. E. 1991 Surface wave and thermocapillary instability in a liquid film flow. *J. Fluid Mech.* **223**, 25–45.

GRIFFITHS, I. M. & HOWELL, P. D. 2008 Mathematical modelling of non-axisymmetric capillary tube drawing. *J. Fluid Mech.* **605**, 181–206.

GUPTA, G. & SCHULTZ, W. W. 1998 Non-isothermal flows of Newtonian slender glass fibers. *Intl J. Non-Linear Mech.* **33**, 151–163.

HU, J., BEN HADID, H. & DANIEL, H. 2008 Linear temporal and spatio-temporal stability analysis of a binary liquid film flowing down an inclined uniformly heated plate. *J. Fluid Mech.* **599**, 269–298.

HUANG, H., MIURA, R. M., IRELAND, W. & PUIL, E. 2003 Heat-induced stretching of a glass tube under tension: application to glass microelectrodes. *SIAM J. Appl. Maths* **63**, 1499–1519.

HUANG, H., MIURA, R. M. & WYLIE, J. J. 2008 Optical fiber drawing and dopant transport. *SIAM J. Appl. Maths* **69**, 330–347.

HUANG, H., WYLIE, J. J., MIURA, R. M. & HOWELL, P. D. 2007 On the formation of glass microelectrodes. *SIAM J. Appl. Maths* **67**, 630–666.

KABOVA, Y. O., KUZNETSOV, V. V. & KABOV, O. A. 2012 Temperature dependent viscosity and surface tension effects on deformations of non-isothermal falling liquid film. *Intl J. Heat Mass Transfer* **55**, 1271–1278.

KAYE, A. 1991 Convected coordinates and elongational flow. *J. Non-Newtonian Fluid Mech.* **40**, 55–77.

KALPAKJIAN, S. & SCHMID, S. R. 2007 *Manufacturing Processes for Engineering Materials*, 5th edn. Prentice Hall.

KALLIADASIS, S., KIYASHKO, A. & DEMEKHIN, E. A. 2003*a* Marangoni instability of a thin liquid film heated from below by a local heat source. *J. Fluid Mech.* **475**, 377–408.

KALLIADASIS, S., DEMEKHIN, E. A. & RUYER-QUIL, C. 2003*b* Thermocapillary instability and wave formation on a film falling down a uniformly heated plane. *J. Fluid Mech.* **492**, 303–338.

KOSTECKI, R., EBENDORFF-HEIDEPRIEM, H., WARREN-SMITH, S. C. & MONRO, T. M. 2014 Predicting the drawing conditions for microstructured optical fiber fabrication. *Opt. Mater. Express* **4**, 29–40.

KUHLMANN, H. C. & RATH, H. J. 1993 Hydrodynamic instability in cylindrical thermocapillary liquid bridges. *J. Fluid Mech.* **247**, 247–274.

MASHAYEK, F. & ASHGRIZ, N. 1995 Nonlinear instability of liquid jets with thermocapillarity. *J. Fluid Mech.* **283**, 97–123.

MATOVICH, M. A. & PEARSON, J. R. A. 1969 Spinning a molten threadline steady-state isothermal viscous flows. *Ind. Engng Chem. Fundam.* **8**, 512–520.

MILADINOVA, S., SLAVTCHEV, S. & LEBON, G. 2002 Long-wave instabilities of non-uniformly heated falling films. *J. Fluid Mech.* **453**, 153–175.

PEARSON, J. R. A. & SHAH, Y. T. 1973 Stability analysis of the fibre spinning process. *Trans. Soc. Rheol.* **16**, 519–533.

ROE, R. J. 1968 Surface tension of polymer liquids. *J. Phys. Chem.* **72**, 2013–2017.

SAMANTA, A. 2008 Stability of liquid film falling down a vertical non-uniformly heated wall. *Physica* D **237**, 2587–2598.

SCHEID, B., RUYER-QUIL, C., THIELE, U., KABOV, O. A., LEGROS, J. C. & COLINET, P. 2005 Validity domain of the Benney equation including the Marangoni effect for closed and open flows. *J. Fluid Mech.* **527**, 303–335.

SEWARD, T. P. III & VASCOTT, T. (Eds) 2005 *High Temperture Glass Melt Property Database for Process Modeling*. The American Ceramic Society, Wiley.

SHAH, Y. T. & PEARSON, J. R. A. 1972*a* On the stability of nonisothermal fibre spinning. *Ind. Engng Chem. Fundam.* **11**, 145–149.

SHAH, Y. T. & PEARSON, J. R. A. 1972*b* On the stability of nonisothermal fibre spinning-general case. *Ind. Engng Chem. Fundam.* **11**, 150–153.

STOKES, Y. M., TUCK, E. O. & SCHWARTZ, L. W. 2000 Extensional fall of a very viscous fluid drop. *Q. J. Mech. Appl. Maths* **53**, 565–582.

STOKES, Y. M. & TUCK, E. O. 2004 The role of inertia in extensional fall of a viscous drop. *J. Fluid Mech.* **498**, 205–225.

STOKES, Y. M., BRADSHAW-HAJEK, B. H. & TUCK, E. O. 2011 Extensional flow at low Reynolds number with surface tension. *J. Engng Maths* **70**, 321–331.

STOKES, Y. M., BUCHAK, P., CROWDY, D. G. & EBENDORFF-HEIDEPRIEM, H. 2014 Drawing of micro-structured fibres: circular and non-circular tubes. *J. Fluid Mech.* **755**, 176–203.

SUMAN, B. & KUMAR, S. 2009 Draw ratio enhancement in nonisothermal melt spinning. *AIChE J.* **55**, 581–593.

TILLEY, B. S. & BOWEN, M. 2005 Thermocapillary control of rupture in thin viscous fluid sheets. *J. Fluid Mech.* **541**, 399–408.

TARONI, M., BREWARD, C. J. W., CUMMINGS, L. J. & GRIFFITHS, I. M. 2013 Asymptotic solutions of glass temperature profiles during steady optical fibre drawing. *J. Engng Maths* **80**, 1–20.

VASILYEV, O. V., TEN, A. A. & YUEN, D. A. 2001 Temperature-dependent viscous gravity currents with shear heating. *Phys. Fluids* **13**, 3664–3674.

VLACHOPOULOS, J. 2003 *The Role of Rheology in Polymer Extrusion, New Technologies for Extrusion Conference*. SPIE Press.

VLACHOPOULOS, J. & POLYCHRONOPOULOS, N. 2012 Basic concepts in polymer melt rheology and their importance in processing. In *Applied Polymer Rheology: Polymeric Fluids with Industrial Applications* (ed. M. Kontopoulou), pp. 1–27. Wiley.

WANG, J. S. & PORTER, R. S. 1995 On the viscosity temperature behavior of polymer melts. *Rheol. Acta* **34**, 496–503.

WEI, H. H. 2005 Thermocapillary instability of core-annular flows. *Phys. Fluids* **17**, 102102.

WU, S. H. 1969 Surface and interfacial tensions of polymer melts: I. Polyethylene, polyisobutylene, and polyvinyl acetate. *J. Colloid Interface Sci.* **31**, 153–161.

WU, S. H. 1970 Surface and interfacial tensions of polymer melts. II. Poly(methyl methacrylate), poly(*n*-butyl methacrylate), and polystyrene. *J. Phys. Chem.* **74**, 632–638.

WILSON, S. D. R. 1988 The slow dripping of a viscous fluid. *J. Fluid Mech.* **190**, 561–570.

WYLIE, J. J. & HUANG, H. 2007 Extensional flows with viscous heating. *J. Fluid Mech.* **571**, 359–370.

WYLIE, J. J., HUANG, H. & MIURA, R. M. 2007 Thermal instability in drawing viscous threads. *J. Fluid Mech.* **570**, 1–16.

WYLIE, J. J., HUANG, H. & MIURA, R. M. 2011 Stretching of viscous threads at low Reynolds numbers. *J. Fluid Mech.* **683**, 212–234.

WYLIE, J. J., HUANG, H. & MIURA, R. M. 2015 Asymptotic analysis of a viscous thread extending under gravity. *Physica* D **313**, 51–60.

YARIN, A. L. 1986 Effect of heat removal on nonsteady regimes of fiber formation. *J. Engng Phys.* **50**, 569–575.

YARIN, A. L., GOSPODINOV, P. & ROUSSINOV, V. I. 1994 Stability loss and sensitivity in hollow fiber drawing. *Phys. Fluids* **6**, 1454–1463.

YIN, Z. L. & JALURIA, Y. 1998 Thermal transport and flow in high-speed optical fiber drawing. *Trans. ASME J. Heat Transfer* **120**, 916–930.

YIN, Z. L. & JALURIA, Y. 2000 Neck down and thermally induced defects in high-speed optical fiber drawing. *Trans. ASME J. Heat Transfer* **122**, 351–362.